nature communications

Article

https://doi.org/10.1038/s41467-025-61047-y

Arginine regulates the mucoid phenotype of hypervirulent *Klebsiella pneumoniae*

Received: 9 December 2024

Accepted: 12 June 2025

Published online: 01 July 2025

Check for updates

Brooke E. Ryan[1], Caitlyn L. Holmes[2], Drew J. Stark[3], Grace E. Shepard[3], Emma G. Mills[3], Saroj Khadka[3], Daria Van Tyne[3], Michael A. Bachman[2] & Laura A. Mike[3]

Hypervirulent *Klebsiella pneumoniae* causes severe community-acquired infections, with its mucoid phenotype resulting from altered capsular polysaccharide chain length. While both environmental and genetic factors influence mucoidy, the cues regulating it remain unclear. Here, we show that casamino acids enhance mucoidy without affecting total capsular polysaccharide levels. We show that arginine is both necessary and sufficient in stimulating mucoid expression, activating the *rmpADC* promoter and increasing *rmpADC* transcript levels. The arginine regulator, ArgR, is crucial in this process; deleting *argR* reduces mucoidy and increases capsule chain length diversity. ArgR directly regulates the *rmpADC* promoter by binding to the ARG box. Loss of *argR* in vitro increases macrophage association and reduces competitive fitness in lungs, suggesting that ArgR influences adherence and fitness in the lung. Arginine-dependent regulation of mucoidy is conserved in hypervirulent *K. pneumoniae* isolates, suggesting that this regulatory mechanism broadly controls bacterial cell surface adaptations.

Klebsiella pneumoniae, a Gram-negative pathogen, ranks as the fourth deadliest bacterial species globally[1]. Hypervirulent *K. pneumoniae* (hvKp) is a concerning pathotype that causes community-acquired outbreaks with high mortality rates[2–5]. While hvKp infections are particularly prevalent in the Asian Pacific Rim, their incidence is spreading worldwide[1,3,5]. This pathotype is quite dangerous due to its capacity to cause severe infections, such as pyogenic liver abscesses, endophthalmitis, and meningitis, even in healthy individuals[2–9]. hvKp isolates are typically hypermucoid and frequently have K1 or K2 capsular serotypes[2,3]. Hypermucoid strains sediment poorly during centrifugation and appear as sticky colonies on LB agar plates.

The *rmp* locus is closely associated with hvKp strains and is found on virulence plasmids or on integrative chromosomal elements (ICEKp)[10]. This locus includes three genes, *rmpA*, *rmpD*, and *rmpC*, where *rmpA* is an autoregulator, *rmpC* positively regulates capsule biosynthetic genes, and *rmpD* regulates the capsular polysaccharide (CPS) chain length[10,11]. Specifically, RmpD binding to the inner membrane protein Wzc decreases the diversity of the CPS chains on the *K. pneumoniae* cell surface[11,12]. These changes in CPS chain length and size distribution shift the bacteria between a mucoid and non-mucoid state. Historically, capsule abundance and mucoidy were considered to be synonymous, however, this perception has evolved. It is now understood that this correlation is likely due to the co-expression of RmpA, RmpC, and RmpD, with RmpD being necessary and sufficient for mucoidy[10–12].

Microenvironments within the host present different nutrient profiles to bacteria. *K. pneumoniae* mucoidy regulation is a complex process influenced by both environmental and genetic factors. Previous research has identified temperature, pH, and certain carbohydrates (*i.e.*, fucose) as regulating mucoidy in *K. pneumoniae*[11,13,14]. For example, urine suppresses hvKp hypermucoidy relative to LB medium by decreasing *rmpD* transcription, while fucose increases it by boosting *rmpD* transcription relative to glucose[11]. However, the specific components in urine that depress *rmpD* and hypermucoidy remain undefined. While temperature, pH, and carbohydrate availability varies across host microenvironments, their effect on

[1]Medical Microbiology and Immunology, University of Toledo, Toledo, OH, USA. [2]Department of Pathology, University of Michigan Medical School, Ann Arbor, MI, USA. [3]Department of Medicine, Division of Infectious Diseases, University of Pittsburgh, Pittsburgh, PA, USA. e-mail: laura.mike@pitt.edu

https://doi.org/10.1038/s41467-025-61047-y

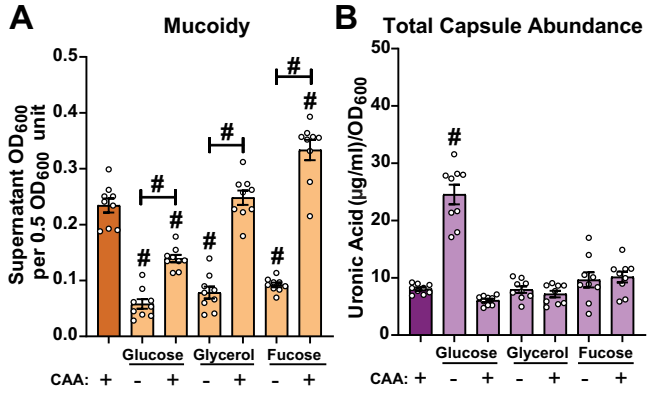

Fig. 1 | Specific nutrients dissociate capsular polysaccharide (CPS) from mucoidy. Wild-type *K. pneumoniae* strain KPPR1 was cultured in low-iron M9 minimal medium with 20 mM glucose (Glc), 20 mM glycerol (Glyc), or 20 mM fucose (Fuc), with or without 1% casamino acids (CAA), as nutrient sources. **A** Mucoidy was determined by quantifying the supernatant OD_{600} after sedimenting 0.5 OD_{600} unit of culture at 1000 x *g* for 5 min. **B** Uronic acid content of crude CPS extracts were quantified and normalized to the OD_{600} of the overnight culture. Data presented are the mean, and error bars represent the standard error of the mean. Statistical significance was determined using a one-way ANOVA with a Tukey post-test. *p*-values are displayed above each comparison, # $p < 0.0001$. The statistics displayed above the data bars represent values relative to M9 + CAA. Statistics connected by lines identify other direct comparisons. Exact *P*-values: (**A**) left to right above data bars: <0.0001, <0.0001, <0.0001, <0.0001, <0.0001; connected by lines: <0.0001, <0.0001, <0.0001; (**B**) left to right: <0.0001. Experiments were performed 3 independent times, each in biological triplicate ($n = 9$). Source data are provided as a Source Data file.

mucoidy in situ during infection remain unclear. In other Gram-negative bacteria, such as *Escherichia coli*, amino acid availability and distribution play essential roles in adaptation, colonization, and proliferation[15]. However, the role of amino acids in regulating mucoidy in *K. pneumoniae* is unexplored despite multiple studies indicating that dysregulation of amino acid metabolism decreases *K. pneumoniae* pathogenesis in multiple in vivo models[16,17]. Understanding how discrete host-derived nutrients modulate mucoidy during *K. pneumoniae* infections is vital for unraveling the mechanisms controlling this virulence-associated phenotype and fine-tuning bacterial fitness during pathogenesis. This is especially important given that bacterial pathogens can adapt to and exploit the metabolic resources available in their host environments to fuel their growth, regulate virulence factors, and optimize fitness[18,19].

Amino acid availability, particularly in tissues like the urinary tract and lungs, plays a critical role in bacterial survival and pathogenesis[15–17]. Specifically, the amino acid arginine exhibits varying concentrations across different host niches, and pathogen responses to these variations are well-documented[15,20,21]. During urinary tract infections (UTIs), amino acids, including arginine, are essential for the growth and survival of uropathogenic *E. coli* (UPEC)[22]. While in the lungs, particularly during a chronic infection, arginine levels can vary significantly compared to that of a healthy lung due to inflammation and immune response. The lung becomes a rich source of metabolites, such as amino acids, when airway defenses are compromised[23]. Specifically, in the sputum of those with cystic fibrosis, arginine is present in millimolar quantities which can serve as a key energy source for bacteria[23,24]. Notably, pathway enrichment analysis has shown that *K. pneumoniae* arginine metabolism is upregulated during a murine lung infection[25].

We and others have observed that *K. pneumoniae*, grown in defined media that was supplemented with casamino acids and glucose, exhibits increased mucoidy compared to growth in defined media with only glucose[14]. In this study, we hypothesized that specific amino acids regulate mucoidy in *K. pneumoniae* by upregulating *rmpD* transcription and altering CPS chain length. Here, we show that arginine is necessary and sufficient to confer the hypermucoid phenotype in hvKp. Further, this arginine-dependent regulation of hypermucoidy is dependent on the regulatory protein, ArgR. Culturing *K. pneumoniae* in arginine-containing medium results in an ArgR-dependent increase in *rmpADC* transcription via the *rmp* promoter, as well as decreased CPS chain length diversity. Arginine-dependent regulation of mucoidy is conserved in five unique hvKp strains, likely due to the highly conserved ARG box found in the *rmp* operon promoter. Mutating the *rmp* promoter ARG box decreases mucoidy, *rmp* promoter activity in multiple hvKp strains, and ArgR binding in vitro. These results support a model where arginine positively controls hypervirulent *K. pneumoniae* mucoidy via ArgR binding to the *rmp* promoter ARG box, increasing *rmpD* expression, and decreasing CPS chain length diversity. Our study highlights a highly conserved pathway regulating one of the primary hvKp virulence factors and represents a potential anti-virulence target.

Results

Casamino acids increase mucoidy without altering total capsule abundance

Specific nutrients that regulate mucoidy without affecting the total capsular polysaccharide (CPS) abundance have not yet been reported. To evaluate the effect of different nutrient sources on *K. pneumoniae* mucoidy and CPS, the hypervirulent strain KPPR1, was cultured in low-iron minimal M9 medium in seven different conditions: 1% casamino acids (M9 + CAA), 20 mM glucose (M9+Glc), 20 mM glucose + 1% casamino acids (M9+Glc+CAA), 20 mM glycerol (M9+Glyc), 20 mM glycerol + 1% casamino acids (M9+Glyc+CAA), 20 mM fucose (M9 + Fuc), and 20 mM fucose + 1% casamino acids (M9+Fuc+CAA). The low-iron condition was used for all M9 media in the entirety of this study as variations in iron availability impact CPS biosynthesis[26]. A standard sedimentation assay was used to quantify mucoidy, while a uronic acid assay was used to quantify total CPS abundance, as glucuronic acid is a major component of *K. pneumoniae* CPS[27]. When amino acids were provided as the primary nutrient source (M9 + CAA) mucoidy was significantly increased compared to M9 supplemented with carbohydrates (Fig. 1A). However, when casamino acids were provided in addition to a carbohydrate, mucoidy increased (Fig. 1A). While M9 + Glc + CAA suppressed mucoidy relative to M9 + CAA, M9 + Fuc + CAA increased mucoidy relative to M9 + CAA (Fig. 1A). Only the M9 + Glyc + CAA condition did not alter mucoidy relative to M9 + CAA(Fig. 1A). Despite these effects on mucoidy, only M9 + Glc significantly increased CPS abundance relative to M9 + CAA (Fig. 1B). Together, these data indicate that *K. pneumoniae* mucoidy and capsule abundance vary independently, with capsule abundance singularly increased by glucose, and mucoidy stimulated in the presence of casamino acids.

Arginine is necessary for the mucoid phenotype

Casamino acids is a mixture of amino acids derived from the acid hydrolysis of casein, a group of phosphoproteins present in mammalian milk. To identify which amino acid(s) in casamino acids confers mucoidy, we prepared a defined low-iron minimal M9 medium supplemented with 20 mM sodium pyruvate and added 18 individual amino acids (M9+All) (Supplementary Data 1). We then generated 18 additional media, each lacking one amino acid (e.g., M9-Arg), to evaluate their individual effects on mucoidy and CPS abundance using sedimentation and uronic acid assays, respectively. We determined that, compared to M9+All, the absence of three individual amino acids (arginine, phenylalanine, or glutamate) resulted in a statistically significant decrease in mucoidy without altering total CPS abundance (Fig. 2A, B). In contrast, the absence of glycine decreased mucoidy and increased CPS abundance (Fig. 2A, B).

https://doi.org/10.1038/s41467-025-61047-y

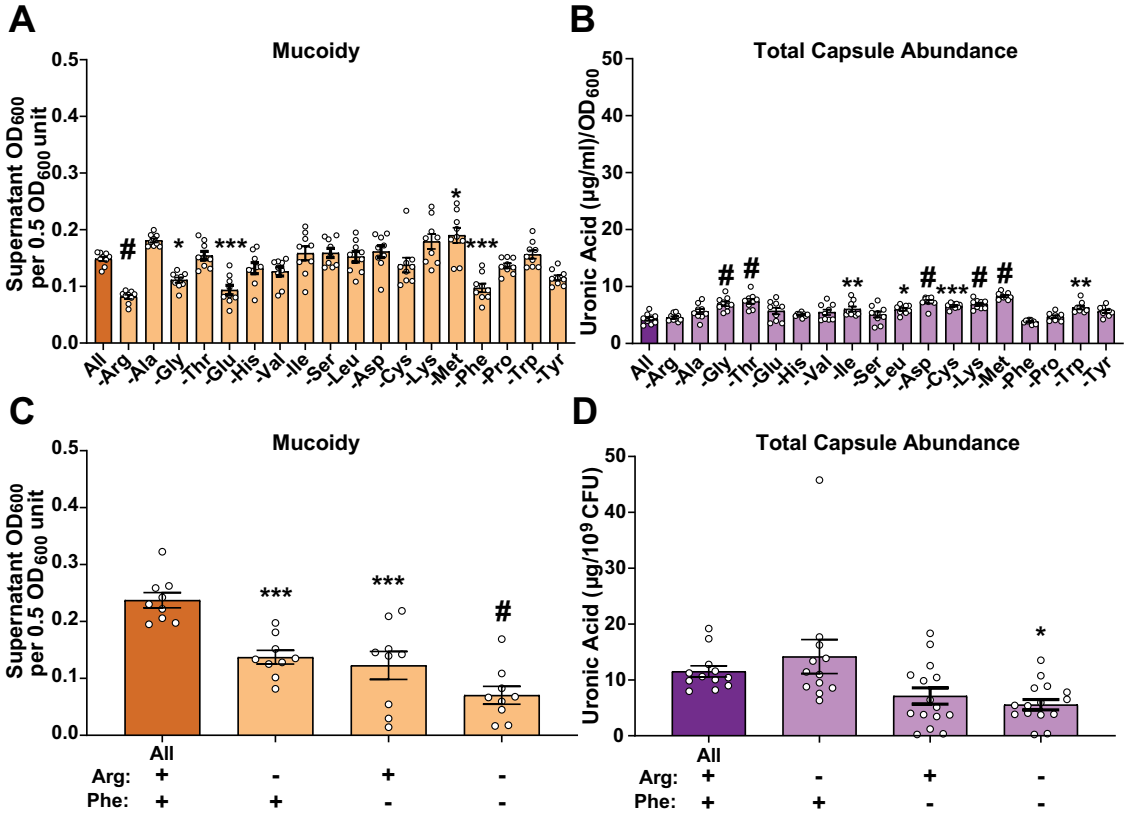

Fig. 2 | Arginine and phenylalanine are necessary for *K. pneumoniae* to regulate mucoidy. Wild type *K. pneumoniae* strain, KPPR1, was cultured in (**A**, **B**) low-iron M9 minimal medium with 20 mM sodium pyruvate and all 18 amino acids (M9 + All), or with an individual amino acid absent. In **C**, **D** KPPR1 was cultured in low-iron minimal M9+All or M9 medium without arginine, or phenylalanine, or with both absent. **A**, **C** Mucoidy was determined by quantifying the supernatant OD_{600} after sedimenting 0.5 OD_{600} unit of culture at 1000 *x g* for 5 min. Uronic acid content of crude CPS extracts were quantified and (**B**) normalized to the OD_{600} of the overnight culture or (**D**) normalized to 10^9 CFUs. Data presented are the mean, and error bars represent the standard error of the mean. Statistical significance was determined using a one-way ANOVA and Dunnett post-test compared to M9 + All. *p*-values are displayed above each comparison; * $p < 0.05$; ** $p < 0.01$; *** $p < 0.001$; # $p < 0.0001$. Exact *P*-values: (**A**) left to right: <0.0001, 0.0350, 0.0002, 0.0131, 0.0008; (**B**) left to right: <0.0001, <0.0001, 0.0077, <0.0001, 0.0001, <0.0001, <0.0001, 0.0013; (**C**) left to right: 0.0007, 0.0001, <0.0001; (**D**) left to right: 0.0470. Experiments were performed ≥ 3 independent times (for graphs A-C, $n = 9$ and for graph d, $n = 9$ for M9 + All and M9-Arg conditions, but $n = 12$ for M9-Phe and M9-Arg-Phe conditions), each in biological triplicate. Source data are provided as a Source Data file.

Sodium pyruvate supplementation was initially included in the M9 medium to aid growth in case the absence of any amino acid impaired growth. However, we found that sodium pyruvate suppresses mucoidy compared to M9 + CAA (Supplementary Fig. 1A). Therefore, when we validated the screening results, we prepared M9 base medium with each amino acid added at the percentage present in casamino acids but did not include the 20 mM sodium pyruvate. This was critical to rule out the possibility that sodium pyruvate itself was masking or modifying the mucoid phenotype. We then prepared four low-iron minimal M9 defined media each lacking a single amino acid identified in Fig. 2A that decreased mucoidy (Arg, Phe, Glu, and Gly). Only the absence of arginine or phenylalanine reproducibly decreased mucoidy (Fig. 2C, D), while the absence of glutamate and glycine did not (Supplementary Fig. 1B). Furthermore, arginine and phenylalanine precursors (Glu or Tyr, respectively) do not contribute to mucoidy individually, or in combination with Arg and Phe (Supplementary Fig. 1B). Ultimately, we found that only arginine absence consistently decreased mucoidy without altering total CPS abundance or growth (Supplementary Fig. 2A–C).

Arginine is sufficient to induce the mucoid phenotype

To determine whether arginine or phenylalanine is sufficient to restore mucoidy, we tested increasing concentrations of arginine and/or phenylalanine in low-iron minimal M9 medium, supplemented with 20 mM glycerol (M9 + Glyc). M9 + Glyc was used to support growth in the absence of any amino acids as it does not suppress mucoidy in the presence of amino acids (Fig. 1A).We performed checkerboard-like assays in 96-well plates to rapidly explore individual and combined effects of arginine and phenylalanine on mucoidy. We discovered that phenylalanine alone is not sufficient to restore mucoidy, and that mucoidy is only restored when arginine is added to M9+Glyc (Supplementary Fig. 3A–C). Based on this screen, we selected optimal arginine concentrations to quantify mucoidy in our standard 3 mL culture volumes. We found that low-iron minimal M9 medium supplemented with 20 mM glycerol and 0.2% arginine (M9+Glyc+Arg) is sufficient to restore mucoidy equivalent to M9+All medium, without altering capsule abundance (Fig. 3A, B). Together, these data indicate that arginine is sufficient to stimulate *K. pneumoniae* mucoidy without altering capsule abundance.

The arginine regulator, ArgR, is required for mucoidy regulation in response to arginine

We next examined the role of genes associated with arginine degradation (*astA*), arginine biosynthesis (*argG*), and arginine regulation (*argR*) in response to exogenous arginine. We used existing KPPR1 *argG::kan* and *astA::kan* transposon mutants and generated a KPPR1 *argR::kan* deletion (Δ*argR*)[16,28–30]. All three strains were cultured overnight in the four media conditions (M9 + All, M9-Arg, M9 + Glyc, and

https://doi.org/10.1038/s41467-025-61047-y

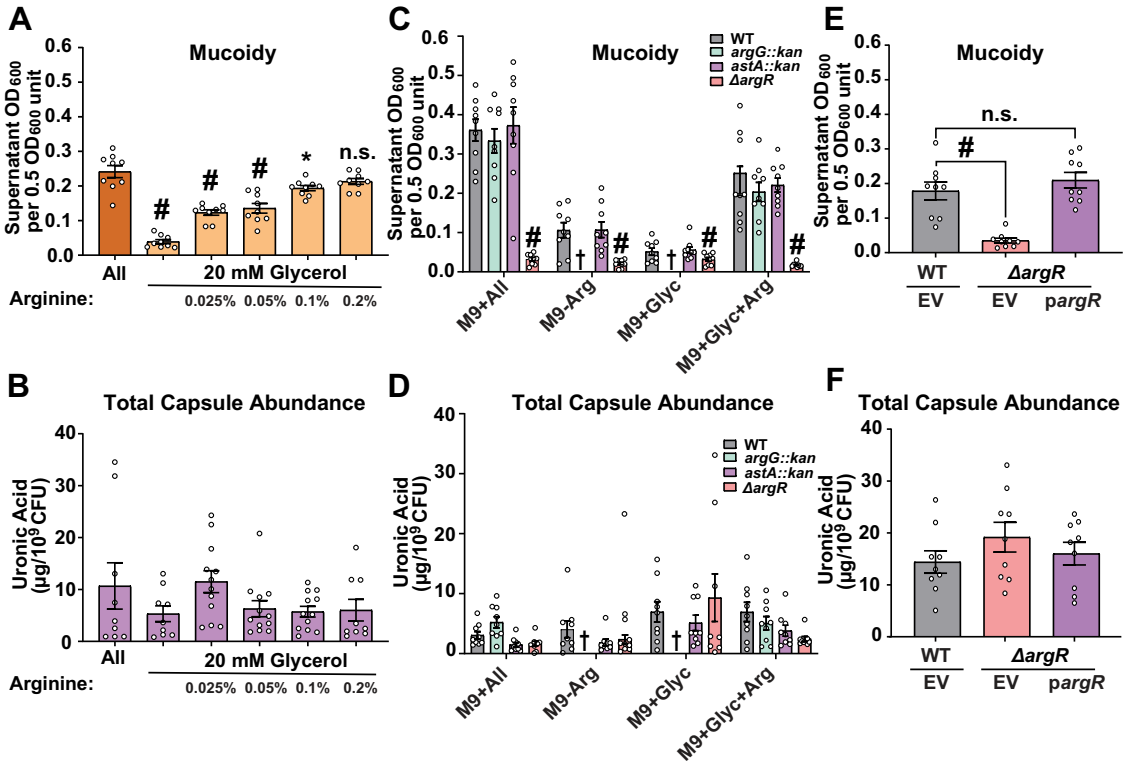

Fig. 3 | Arginine is sufficient to induce mucoidy in *K. pneumoniae* and requires the ArgR regulator. A, **B** Wild-type (WT) KPPR1 was cultured overnight in low-iron M9 medium supplemented with 18 amino acids (All), 20 mM glycerol (Glyc), or increasing concentrations of arginine (0.025%–0.2%) and 20 mM Glyc. **C**, **D** Additionally, KPPR1, *astA*::kan, *argG*::kan, and Δ*argR* mutants were cultured overnight in low-iron M9 minimal media under the following conditions: with 18 amino acids (All), without arginine (-Arg), with 20 mM glycerol (Glyc), or with 20 mM glycerol and 0.2% arginine (Glyc+Arg). (**E**, **F**) The strains KPPR1 and Δ*argR* were transformed with either the empty vector (EV) or *argR* vector (p*argR*) and cultured overnight in low-iron minimal M9+All medium. **A**–**E** Mucoidy was determined for each of the conditions by sedimenting 0.5 OD_{600} unit of culture at 1000 x *g* for 5 min and then measuring the supernatant OD_{600}. **B**–**F** The total capsule abundance was determined by measuring the uronic acid content of crude CPS extracts and normalized to 10^9 CFUs. Data presented are the mean, and error bars represent the standard error of the mean. In panels (**C**, **D**) the cross (†) indicates no growth. **A**–**F** Statistical significance was determined using one-way ANOVA with a Dunnett post-test. **C**, **D** Statistical significance was determined using two-way ANOVA with a Tukey post-test. The statistics indicated above the data bars represent values relative to M9 + All (**A**, **B**) or WT in the same culture condition (**C**–**F**). *p*-values are displayed above each comparison; * $p < 0.05$; # $p < 0.0001$. Exact *P*-values: (**A**) left to right: <0.0001, <0.0001, <0.0001, 0.0135; (**C**) left to right: <0.0001, <0.0001, <0.0001, <0.0001; (**E**) left to right: <0.0001. Experiments were performed 3 independent times, each in biological triplicate (for graphs A,C-F, $n = 9$ and for graph B, $n = 9$ for M9 + All, M9+Glyc, and 0.2% arginine conditions, but $n = 12$ for 0.025%-0.1% arginine conditions). Source data are provided as a Source Data file.

M9 + Glyc + Arg) and mucoidy was then assessed by sedimentation assay, except *argG::kan* which cannot grow in the absence of arginine (M9-Arg, M9 + Glyc). Δ*argR* exhibited significantly reduced mucoidy compared to wild-type (WT) KPPR1 in all tested media (Fig. 3C). The *argG::kan* and *astA::kan* transposon mutants had no significant mucoidy differences in any tested media. Capsular polysaccharide abundance was unchanged for any of the mutants, indicating that the effects of Δ*argR* on mucoidy are independent of total capsule abundance (Fig. 3D). Compared to WT KPPR1, there were no defects in the maximum endpoint OD_{600} in any of the mutants in M9+All, except *argG::kan* had a growth defect based on area under the curve (Supplementary Fig. 4A–C). However, since mucoidy is measured at the 16 h endpoint and all strains have the same OD_{600} at that timepoint, the observed changes in mucoidy are likely not due to growth defects.

To verify that ArgR is solely responsible for the observed effects on mucoidy, we generated a complementation vector expressing *argR* driven by the native *argR* promoter (p*argR*). As expected, p*argR* fully complemented Δ*argR* loss-of-mucoidy and did not alter total capsule abundance (Fig. 3E, F). These results indicate that arginine degradation and biosynthesis are not required to regulate mucoidy, but the ArgR regulator is required for KPPR1 to up-regulate the mucoid phenotype in response to exogenous arginine.

Arginine increases *rmpADC* promoter activity and transcription in an ArgR-dependent manner

To determine how arginine and ArgR alter mucoidy status, we examined whether arginine stimulates *rmpADC* promoter (P_{rmp}) activity by using a GFP reporter plasmid (P_{rmp}-*dasherGFP*). KPPR1 carrying P_{rmp}-*dasherGFP* was cultured in either M9 + All, M9-Arg, M9 + Glyc, or M9 + Glyc + Arg medium, and GFP fluorescence was measured and normalized to OD_{600}. P_{rmp} activity decreased when the reporter strain was cultured in M9-Arg medium (non-mucoid), relative to M9+All medium (Fig. 4A). Conversely, P_{rmp} activity was increased when the reporter strain was cultured in M9 + Glyc + Arg medium (mucoid) relative to M9 + Glyc medium (Fig. 4A). P_{rmp} activity was low in the Δ*argR* mutant, regardless of arginine availability (Fig. 4A).

As we and others have shown, *rmpD* transcript levels correlate with mucoidy levels due to RmpD modulating Wzc function to increase CPS chain length and uniformity[11,12]. To directly examine the effects of arginine availability on *rmpADC* transcription, we quantified *rmpA*, *rmpD*, *rmpC*, and *gap2* (internal control) transcript abundance in KPPR1 cultured in the four same media conditions (M9+All, M9-Arg, M9+Glyc, and M9+Glyc+Arg). In M9-Arg medium (non-mucoid), the *rmpADC* transcripts are significantly decreased compared to M9+All medium (Fig. 4B). Additionally, in M9+Glyc+Arg medium (mucoid), *rmpADC* transcripts are significantly increased compared to M9+Glyc

https://doi.org/10.1038/s41467-025-61047-y

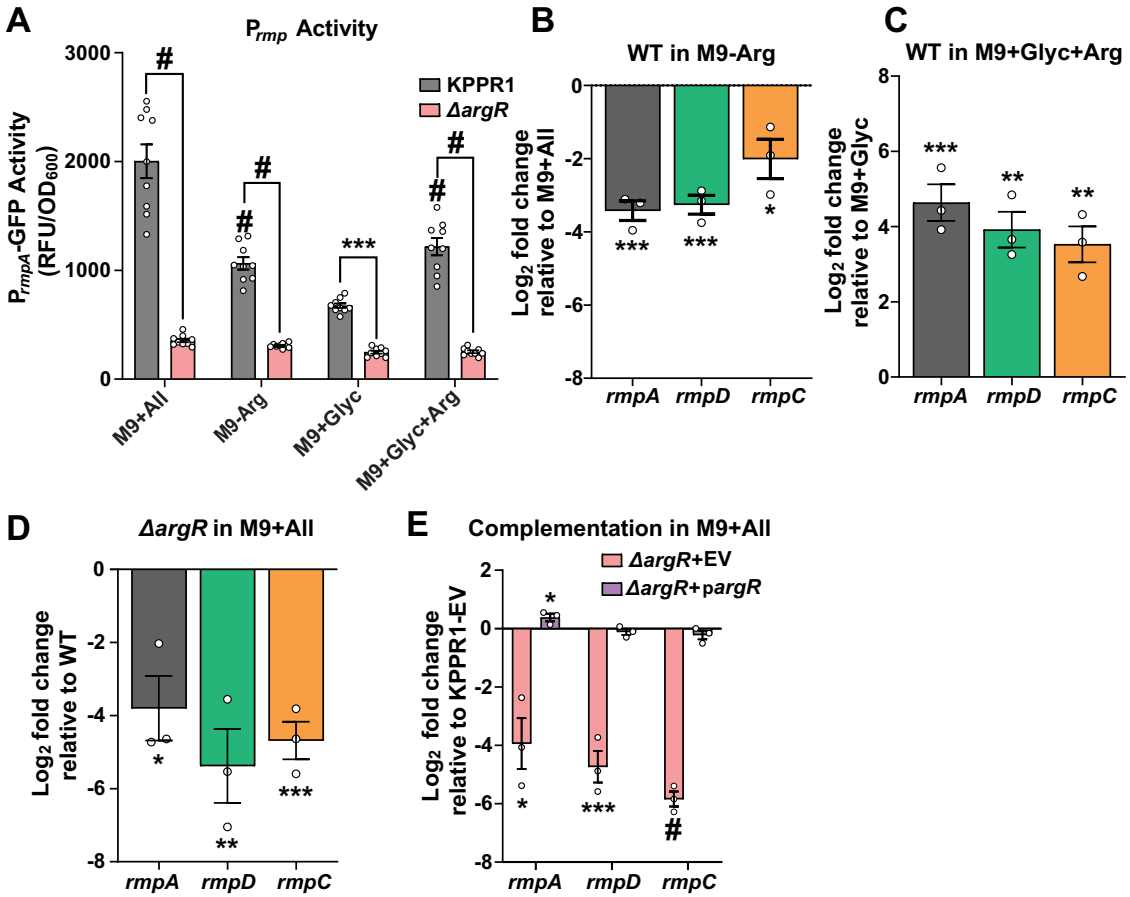

Fig. 4 | Arginine regulates mucoidy by increasing *rmpADC* transcription in an ArgR-dependent manner. KPPR1 and the Δ*argR* mutant were cultured under different amino acid conditions (M9 + All, M9-Arg, M9 + Glyc, M9 + Glyc + Arg). **A** *Rmp* promoter (P_{rmp}) activity was measured by GFP expression via a promoter fusion. RNA was isolated from mid-log cultures of KPPR1 in the four media or from Δ*argR* and the complementation vectors (KPPR1 + EV, *argR* + EV, or *argR*+p*argR*) in M9 + All. **B**–**E** The relative abundance of *rmpA*, *rmpD*, and *rmpC* RNA under the different conditions was determined by qRT-PCR and normalized to *gap2* transcript abundance. **B**, **C** Relative transcript levels in KPPR1 cultured in M9-Arg or M9+Glyc +Arg were compared to M9 + All or M9 + Glyc, respectively, while (**D**) the Δ*argR* mutant (cultured in M9 + All) transcript levels were compared to wildtype, KPPR1. (**E**) The complementation transcript levels were compared to KPPR1 + EV. Data presented are the mean, and error bars represent the standard error of the mean. Statistical significance was determined in panel (**A**) with a two-way ANOVA with Tukey's post-test. The statistics displayed above the data bars represent values relative to M9 + All. Statistics connected by lines identify other direct comparisons. In panels (**B**–**E**) significance was determined using a two-tailed unpaired *t*-test to determine. *p*-values are displayed above each comparison; $^{*}p < 0.05$; $^{**}p < 0.01$; $^{***}p < 0.001$; # $p < 0.0001$. Exact *P*-values: (**A**) left to right above data bars: <0.0001, <0.0001; connected by lines: <0.0001, <0.0001, 0.0005, <0.0001; (**B**) left to right: 0.0002, 0.0002, 0.0199; (**C**) left to right: 0.0007, 0.0012, 0.0018; (**D**) left to right: 0.0127, 0.0060, 0.0008; (**E**) left to right: 0.0107, 0.0398, 0.0009, <0.0001. Experiments were performed ≥ 3 independent times (for graph A, $n = 9$ with biological replicates and for graph B-E, $n = 3$ with technical replicates). Source data are provided as a Source Data file.

(Fig. 4C). In agreement with the positive effect of exogenous arginine on *rmpADC* transcripts abundance, the Δ*argR* mutant had a significant decrease in *rmpADC* transcripts relative to WT KPPR1 (Fig. 4D). This ArgR-dependent loss of *rmpADC* transcripts was fully complemented by p*argR* (Fig. 4E). No other candidate amino acids or genes changed *rmpD* transcript levels (Supplementary Fig. 4F; Supplementary Fig. 5A). These results indicate that the presence of arginine increases mucoidy by increasing P_{rmp} activity and *rmpADC* transcription in an ArgR-dependent manner.

Arginine and ArgR decrease capsular polysaccharide chain diversity

Recently, our lab and others reported that diverse, shorter CPS chains are associated with a non-mucoid colony phenotype while uniform, longer CPS chains are associated with a hypermucoid phenotype[11,12]. RmpD interacts with the chain-length-regulating tyrosine autokinase, Wzc, to increase CPS chain length and uniformity[11,12]. Therefore, we examined the effects of arginine and ArgR on CPS chain length diversity. Cell-associated CPS was isolated from WT KPPR1 cultured in M9+All, M9-Arg, M9 + Glyc, or M9 + Glyc + Arg normalized to an OD_{600} of 1.5[27]. The cell-associated CPS was resolved by SDS-PAGE and visualized using Alcian blue and then silver stain[27]. When KPPR1 is cultured in LB medium the bacteria appear mucoid and produce three distinct polysaccharide bands, corresponding to CPS species that we previously described as Type A (diverse; mid- to high-molecular weight chains), Type B (uniform; high-molecular weight chains), and Type C (ultrahigh-molecular weight chains)[11]. When arginine is absent from the media, the diverse Type A CPS chains that appear as a smear on the gel increase significantly, while when arginine is added to the media, the diverse Type A CPS chains decrease and uniform Type B CPS chains increase significantly (Fig. 5A–D). We evaluated the CPS chain length diversity of WT and Δ*argR* cultured in M9+All medium, as we observed the strongest mucoid phenotype differences in this culture medium (Fig. 3C). The Δ*argR* strain produced significantly more Type A CPS chains, and decreased Type B and Type C CPS chains, thereby increasing overall cell surface CPS chain length diversity

https://doi.org/10.1038/s41467-025-61047-y

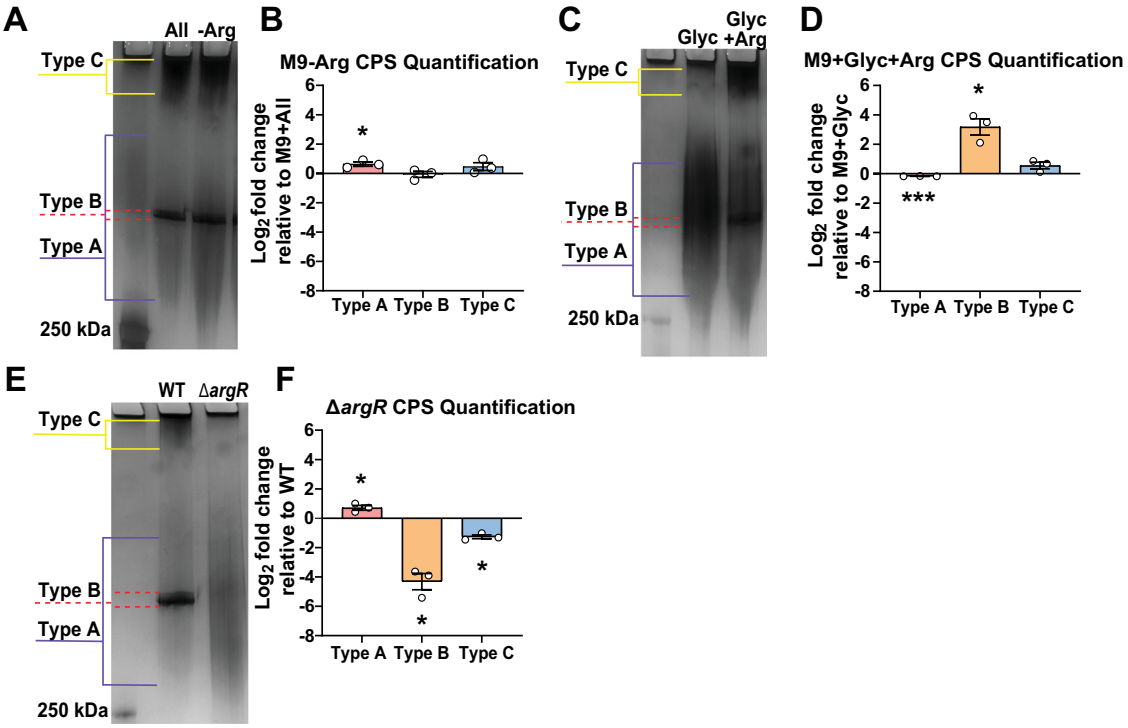

Fig. 5 | Arginine and ArgR regulate mucoidy by increasing *rmpD* transcription and decreasing capsular polysaccharide chain length diversity. KPPR1 and the Δ*argR* mutant were cultured in different amino acid conditions (M9 + All, M9-Arg, M9 + Glyc, M9 + Glyc + Arg) or (M9 + All), respectively. **A**, **C**, **E** Capsular polysaccharides (CPS) were separated on a 4-15% SDS-PAGE gel and stained with Alcian blue and silver stain. Three distinct polysaccharide types emerged: diverse mid- to high-molecular-weight chains (Type A), uniform high-molecular-weight chains (Type B), and diffuse ultra-high-molecular-weight chains (Type C). Data presented are the mean, and error bars represent the standard error of the mean. Representative images of the three independent gels are shown in panels (**A**, **C** and **E**) with the quantification of three independent replicates being shown in panels (**B**, **D**, and **F**) ImageJ was used to quantify each CPS chain type with background subtracted. To minimize gel-to-gel variability, the control and experimental density values were extracted from the same gel and used to calculate fold-change abundance. Changes in CPS type production were determined by calculating the fold-change in experimental density values relative to control density values on three independent gels. Statistical significance was determined using a two-tailed one sample *t*-test. *p*-values are displayed above each comparison; * $p < 0.05$; *** $p < 0.001$. Exact *P*-values: (**B**) left to right: 0.0474; (**D**) left to right: 0.0010, 0.0289; (**F**) left to right: 0.0488, 0.0161, 0.0107. Experiments were performed ≥ 3 independent times ($n = 3$). Source data are provided as a Source Data file.

compared to WT KPPR1 (Fig. 5E, F). No other candidate amino acids or tested genes altered capsule chain length diversity (Supplementary Fig. 4D, E; Supplementary Fig. 5B, C). These results indicate that the presence of arginine decreases Type A CPS abundance, increasing the overall uniformity of the cell-associated CPS chains and increasing the mucoid phenotype, in an ArgR-dependent manner.

We previously reported that Wzc phospho-status is sometimes reduced by Wzc mutations that increase mucoidy and Types B and C polysaccharide production[11]. Therefore, we also determined whether the absence of arginine or phenylalanine affects Wzc phospho-status[11]. KPPR1 was cultured in M9+All, M9-Arg, M9-Phe, and M9-Arg-Phe and whole-cell lysates were prepared and separated by SDS-PAGE. The phosphotyrosine profiles in each growth condition were analyzed by western blot and we found Wzc phosphorylation is only decreased when neither arginine nor phenylalanine are present (Supplementary Fig. 5D, E). Although the literature supports that Wzc phosphocycling directs CPS chain length regulation, our findings suggest that Wzc phosphorylation status is unlikely to be a good indicator of CPS chain length diversity regulation. It is possible that monitoring the kinetics (as opposed to static level) of Wzc phosphorylation may provide more insight into the regulation of CPS chain length diversity. Altogether, our data indicate that arginine and ArgR decrease CPS chain length diversity by boosting RmpD levels. Therefore, we propose a model in which arginine reduces CPS chain length diversity via RmpD-dependent Wzc modulation rather than altering Wzc phosphorylation state.

ArgR reduces macrophage association and enhances bacterial fitness in the lung

Since mucoidy has been previously reported to interfere with *K. pneumoniae* association with macrophages and epithelial cells, we next quantified how effectively the Δ*argR* strain adheres to immortalized bone marrow-derived macrophages from *Mus musculus* (iBMDMs, BEI #NR-9456)[11,12,30,31]. We first evaluated KPPR1 and Δ*argR* mucoidy in LB and DMEM media to identify if the assay conditions altered strain behavior. We found that the mucoid phenotypes of KPPR1 and Δ*argR* in LB and DMEM matched mucoidy patterns observed in M9 + All (Supplementary Fig. 6A, 6B). We then found that total Δ*argR* mutant CFUs bound to and internalized by macrophages was 4.3-fold greater than WT ($P < 0.0001$), while intracellular Δ*argR* mutant CFUs was 2.3-fold greater than WT ($P = 0.0287$) (Fig. 6A). To determine the effects of an *argR* deletion during infection, we competed WT + EV (EV = empty vector) against Δ*argR* + EV or Δ*argR* + p*argR* (the complemented strain) in a murine pneumonia model and bacterial burdens were enumerated after 24 h (Fig. 6B and Supplementary Fig. 6C, D). As predicted, Δ*argR* + EV was outcompeted 2.5 log-fold by WT + EV ($P = 0.0008$), while the Δ*argR* + p*argR* not only complemented the competitive defect in the lungs seen by Δ*argR* + EV ($P < 0.0001$) but had enhanced lung fitness relative to WT + EV (Fig. 6B). There was no significant fitness defect of Δ*argR* + EV in the spleen or liver. There was a significant decrease in the competitive index (CI) of Δ*argR* + p*argR* in the spleen, although this was not significantly different than the CI of Δ*argR* + EV. Taken together, these data strongly suggest that ArgR activity

https://doi.org/10.1038/s41467-025-61047-y

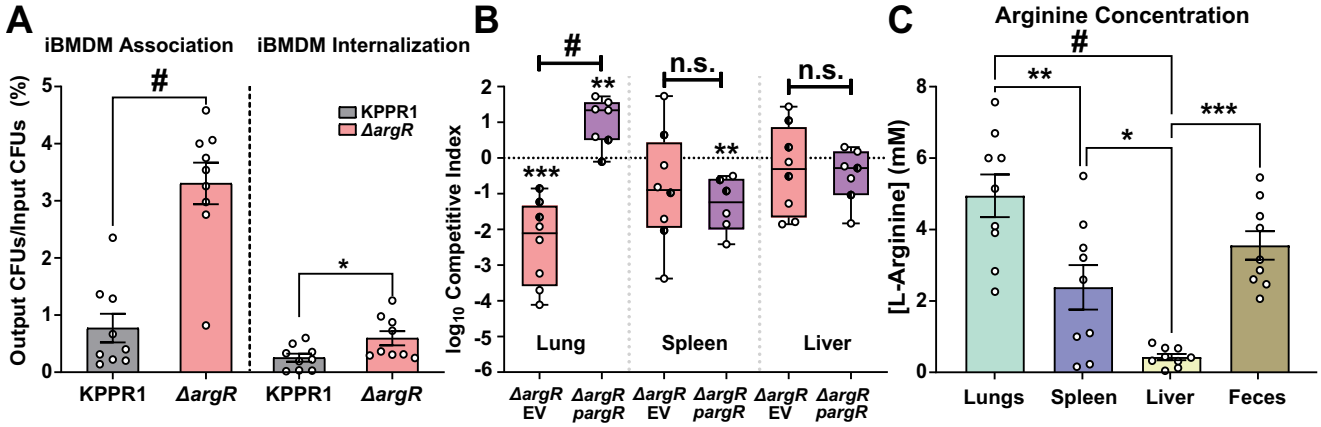

Fig. 6 | ArgR is required for *K. pneumoniae* to evade immortalized bone marrow-derived macrophages (iBMDMs) association and maintain competitive fitness in the lung. A Macrophages (BEI NR-9456) were incubated with KPPR1 or Δ*argR* for 2 hr (MOI = 10). Internalization was determined by a 1 hr gentamicin treatment. Macrophages were washed with PBS, lysed with 0.2% TritonX100, and output CFUs were enumerated and normalized to input. Experiments were performed > 3 independent times, in triplicate ($n = 9$). Data presented are the mean, and error bars represent the standard error of the mean. **B** C57BL/6 mice were infected retropharyngeally with 1×10^6 CFUs of a 1:1 mixture of WT + EV and either Δ*argR* + EV or Δ*argR* + p*argR*. The $\log_{10}$ competitive index at 24 h post-infection is shown relative to 0. Each dot represents an individual mouse (open symbols = male; half-filled = female). The horizontal line represents the median; box bounds indicate the minima (25TH percentile) and maxima (75TH percentile); and whiskers represent the full range. Δ*argR* + EV was tested in two independent experiments ($n = 8$), while Δ*argR*+p*argR* was tested once ($n = 7$). **C** Arginine concentrations were measured in murine lungs, spleens, livers, and feces. Samples were collected from three mice and experiments were performed 3 independent times, in technical triplicate ($n = 3$). Data presented are the mean, and error bars represent the standard error of the mean. Statistical significance was determined using an unpaired two-tailed *t*-test (**A**), a two-tailed unpaired *t*-test (**B**, comparing CI values between Δ*argR* + EV and Δ*argR*+p*argR*), and a two-tailed one-sample *t*-test (**B**, comparing CI to a hypothetical value of zero). In (**C**), a one-way ANOVA with Tukey's post-test was used. *p*-values are displayed above each comparison; $^*p < 0.05$; $^{**}p < 0.01$, $^{***}p < 0.001$; $\#p < 0.0001$. Exact *P*-values: (**A**) left to right: <0.0001, 0.0287; (B) left to right above data bars: 0.0008, 0.0078, 0.0081; connected by lines: <0.0001; (**C**) left to right: 0.0033, <0.0001, 0.0327, 0.0003. Source data are provided as a Source Data file.

decreases bacterial adherence to and internalization by host immune cells and is necessary for bacterial fitness in the lungs.

We next wanted to measure local arginine concentrations in sites of infection and colonization. To do this, we quantified arginine abundance in homogenized murine lungs, spleen, and liver. In addition, ArgR was recently reported to regulate hvKp T6SS, which is required for gut colonization[32]. Therefore, we also quantified arginine concentration in murine feces[14,32]. We measured arginine concentrations after proteinase-treating homogenized host tissues. We found that murine lungs had 11.6-fold ($P < 0.0001$), and 2-fold ($P = 0.0033$) higher arginine concentrations compared murine liver and spleen, respectively (Fig. 6C). The murine feces had 8.3-fold ($P = 0.0003$) higher arginine concentration compared to murine liver. The higher arginine concentrations in murine lungs and feces suggest that these may be arginine-replete niches for hvKp, while the liver may be an arginine-deprived environment. Taken together, these data suggest that ArgR-dependent regulation may vary in different host niches occupied by hvKp.

ArgR regulates the *rmp* promoter by binding to a highly conserved ARG box

ArgR is activated by arginine and binds to regulatory targets via an ARG box. Therefore, we next examined whether there was a predicted ARG box in P_{rmp} of KPPR1. We identified an ARG box in the *rmp* promoter region of *K. pneumoniae*, which contains eighteen nucleotides. Notably, eight of those nucleotides are highly conserved in other reported *K. pneumoniae* ARG boxes. (Fig. 7A, asterisks)[33]. Expanding our analysis to 1572 publicly available genomes, we found 100% conservation of the ARG box across all hypervirulent strains (Fig. 7A).

To determine if the ARG box is essential for arginine-dependent regulation, we mutated the eight conserved nucleotides in P_{rmp} on the reporter plasmid to make $P_{rmp\Delta ARG}$-dasherGFP (Fig. 7A, asterisks). WT KPPR1 carrying P_{rmp} and $P_{rmp\Delta ARG}$ reporter plasmids were cultured in M9 + All, M9-Arg, M9 + Glyc, or M9 + Glyc + Arg medium, and we measured GFP fluorescence as before. GFP expression from $P_{rmp\Delta ARG}$-dasherGFP was decreased in all media compared to KPPR1 P_{rmp}-dasherGFP (Fig. 7B). Next, to determine if ArgR directly binds the *rmp* promoter (P_{rmp}) via the ARG box, we performed a DNA-protein interaction enzyme-linked immunosorbent assay (DPI-ELISA)[32,34]. We synthesized DNA oligonucleotides containing the ARG box in P_{rmp} or with the eight conserved nucleotides mutated in the ARG box ($P_{rmp\Delta ARG}$). ArgR binds $P_{rmp\Delta ARG}$ significantly less compared to P_{rmp} (Fig. 7C).

To confirm the direct role of the P_{rmp} ARG box in arginine-dependent activation of mucoidy, we made a chromosomal ARG box mutation (ΔARGbox) in KPPR1S to assess the effects on mucoidy and *rmpADC* transcription[35]. We cultured the ΔARGbox mutant strain in M9 + All, M9-Arg, M9 + Glyc, or M9 + Glyc + Arg medium and quantified mucoidy as described earlier. The ΔARGbox mutant exhibited decreased mucoidy across all media compared to KPPR1S (Fig. 7D) but increased total capsule abundance in all media compared to KPPR1S (Fig. 7E). The increased total capsule abundance in the ΔARGbox mutant compared to the Δ*argR* strain could be due to ArgR influencing capsule abundance distinct from its control of the *rmp* locus. These results mirror the Δ*argR* mucoidy phenotype (Fig. 3C), supporting our model that the ARG box is required for the control of mucoidy by ArgR in response to arginine.

To determine if the ΔARGbox mutant reduces mucoidy by decreasing *rmpADC* transcripts, we cultured the ΔARGbox mutant strain in M9+All medium, as done previously for Δ*argR* (Fig. 4D), and quantified *rmpA*, *rmpD*, *rmpC*, and *gap2* (internal control) transcript abundance. We found that the ΔARGbox mutant strain had significantly decreased *rmpA*, *rmpD*, and *rmpC* transcript levels compared to KPPR1S (Fig. 7F). Additionally, to evaluate if the decreased mucoidy of the ΔARGbox mutant is driven by increased capsule chain length diversity, we cultured the ΔARGbox mutant strain in M9+All medium and visualized purified CPS by SDS-PAGE. We found that the ΔARGbox mutant significantly decreased Type C

https://doi.org/10.1038/s41467-025-61047-y

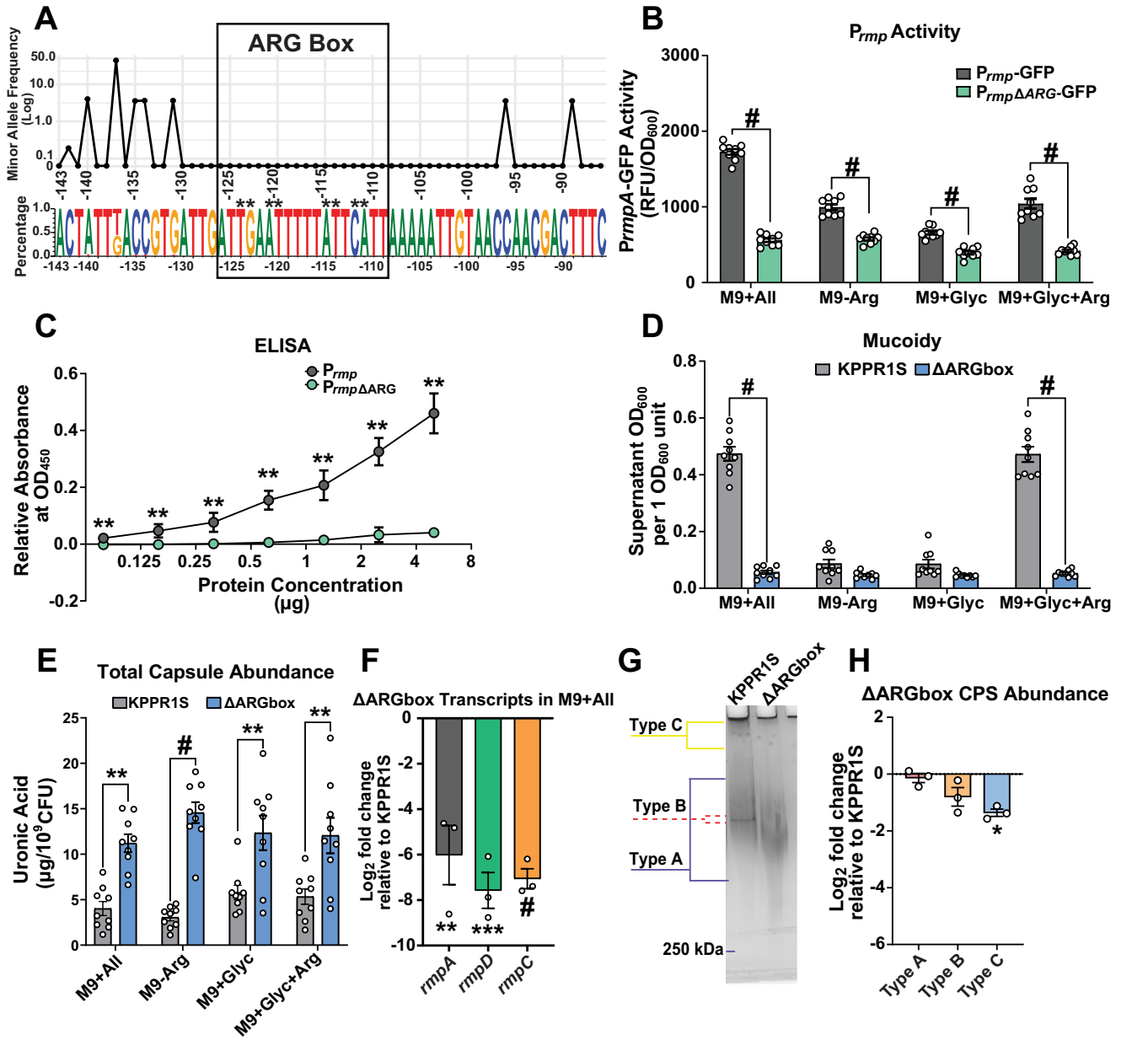

Fig. 7 | A highly conserved ARG box in the *rmp* promoter is required for ArgR-dependent mucoidy regulation. A *K. pneumoniae* genomes with intact *rmpADC* loci ($n = 1572$) were analyzed for ARG box sequence diversity using Geneious v2023.1.1 and WebLogo v3.7.9. Diversity is shown as percentage and minor allele frequency. Asterisks indicate highly conserved nucleotides. **B** KPPR1 carrying either a P$_{rmp}$-GFP reporter plasmid or a mutated ARG box (P$_{rmp\Delta ARG}$-GFP) was cultured in M9 + All, M9-Arg, M9 + Glyc, or M9 + Glyc + Arg. GFP expression measured promoter activity. **C** DNA-protein interaction ELISA assessed ArgR binding to the ARG box in P$_{rmp}$. Purified His$_6$-tagged ArgR was incubated in wells coated with DNA oligomers containing either the predicted (P$_{rmp}$) or mutated binding site (P$_{rmp\Delta ARG}$). Binding was detected using an HRP-conjugated anti-poly-histidine antibody. OD$_{450}$ values reflect ArgR-DNA binding. **D**, **E** KPPR1S or chromosomal ARG box mutant (ΔARGbox) were cultured in the four media conditions. **D** Mucoidy was assessed by sedimentation assay. **E** Capsule abundance was measured by uronic acid quantification. **F**–**H** KPPR1S and ΔARGbox mutant were cultured in M9+All. **F** Transcript levels of *rmpA*, *rmpD*, and *rmpC* were measured by qRT-PCR and normalized to *gap2*. **G** Capsular polysaccharides (CPS) were separated by SDS-PAGE and stained with Alcian blue and silver stain; representative image of three independent gels shown. **H** Quantification was done with ImageJ with background subtraction. Data presented are the mean, and error bars represent SEM. Statistical tests: unpaired two-tailed *t*-test (**B**, **F**); two-tailed Mann-Whitney test (**C**); two-way ANOVA with Bonferroni's post-test (**D**, **E**); two-tailed one sample *t*-test (**H**). *p*-values: $^{**}p < 0.01$; $\#p < 0.0001$. Exact *P*-values left to right: (**B**): <0.0001, <0.0001, <0.0001, <0.0001; (**C**): 0.0087, 0.0022, 0.0022, 0.0022, 0.0022, 0.0022, 0.0022; (**D**): <0.0001, <0.0001; (**E**): 0.0025, <0.0001, 0.0085, 0.0061; (**F**): 0.0098, 0.0007, <0.0001; (**H**): 0.0188. Experiments were performed > 3 independent times ($n = 9$), in triplicate, except (**G**) ($n = 3$) and (**C**) (duplicates, $n = 6$). Source data are provided as a Source Data file.

CPS chains and trended towards decreased abundance of the uniform, Type B CPS chains (Fig. 7G, H). Together, these results demonstrate that the highly conserved ARG box in the *rmp* promoter is essential for arginine-dependent regulation of mucoidy via ArgR.

Arginine-dependent regulation of mucoidy occurs in multiple hypervirulent K. pneumoniae isolates and host environments

Based on the broad conservation of the predicted ARG box in hypervirulent *K. pneumoniae* strains, we next sought to determine whether arginine-dependent regulation of mucoidy is conserved in four

additional hvKp strains. While the mucoidy data thus far was collected using the hvKp strain KPPR1, we expanded our analysis to include other hvKp strains, namely, the laboratory strain NTUH-K2044 and three clinical isolates: Kp4289, Kp4585, and Kp6557[36]. All strains were confirmed to genetically encode *rmp* with PathogenWatch (Table 1)[37–43]. To evaluate if P_{rmp} activity was similarly regulated in the clinical isolates, we introduced P_{rmp}-GFP and $P_{rmp\Delta ARG}$-GFP reporter plasmids into all four hvKp strains, then measured GFP fluorescence in M9+All and M9-Arg. Three of the four strains exhibited reduced P_{rmp}-GFP expression in M9-Arg relative to M9+All (Fig. 8A). However, in all conditions, GFP expression was significantly decreased in all strains carrying $P_{rmp\Delta ARG}$ compared to the strains carrying P_{rmp} (Fig. 8A). Together, these data suggest that the positive regulation of mucoidy by arginine-dependent regulation of the *rmp* promoter occurs in multiple hvKp strains. To evaluate whether mucoidy was increased by arginine in these four hypervirulent strains, the strains were cultured in M9+All or M9-Arg and mucoidy was quantified by sedimentation assay. In agreement with our model, we observed a significant increase in mucoidy in all strains when cultured in M9+All relative to arginine-free medium (M9-Arg) (Fig. 8B).

We next wanted to evaluate whether hvKp could up- or down-regulate mucoidy in response to varying arginine concentrations in more complex environments. To do this, we quantified arginine abundance in human urine and human serum, and then correlated those data with hvKp mucoidy and *rmpADC* promoter activity. We measured arginine concentrations in these two proteinase-treated environments and found that human urine contained 6.2-fold ($P < 0.0001$) less arginine than low-iron minimal M9 medium with 20% heat-inactivated serum (M9 + HI Serum) (Fig. 8C). We evaluated the effect of human urine and serum on *rmpADC* promoter activity by culturing KPPR1 carrying P_{rmp} or $P_{rmp\Delta ARG}$ in human urine and M9 + HI Serum. GFP expression was reduced by 1.41-fold ($P = 0.0138$) in human urine compared to M9 + HI Serum in strains carrying P_{rmp}-GFP (Fig. 8D). The level of GFP expression was reduced 2.0-fold ($P < 0.0001$) in KPPR1 carrying $P_{rmp\Delta ARG}$ relative to P_{rmp} cultured in M9 + HI Serum, suggesting that arginine available in human serum up-regulates P_{rmp} activity. Finally, we assessed if changes in promoter activity corresponded to alterations in mucoidy by culturing both KPPR1 and Δ*argR* strains in human urine and M9 + HI Serum and measuring mucoidy. KPPR1 mucoidy was 2.07-fold ($P < 0.0001$) lower when cultured in human urine compared to M9 + HI Serum (Fig. 8D). The Δ*argR* strain exhibited a 1.78-fold ($P < 0.0001$) reduced mucoidy compared to KPPR1 in M9 + HI Serum only. Taken together, these results indicate that arginine levels in human biofluids can influence hypervirulent *K. pneumoniae rmp* promoter activity and alter mucoidy in an ArgR- and ARG box-dependent manner.

Discussion

K. pneumoniae mucoidy is influenced by both environmental conditions and genetic factors, with arginine emerging as a key modulator of this phenotype. Our results reveal that ArgR positively regulates *K. pneumoniae* mucoidy (Fig. 3C) in response to arginine availability (Fig. 3A) by binding to the ARG box in the promoter of *rmpADC* (Fig. 7), increasing expression of the *rmpADC* operon (Fig. 4), producing less diverse CPS chains (Fig. 5), decreasing association with macrophages and fitness in the lung (Fig. 6), and increasing mucoidy in hypervirulent *K. pneumoniae* strains and different host environments (Fig. 8B, D). While casamino acids significantly increase mucoidy, they do not alter the overall total capsular polysaccharide abundance (Fig. 1A, B). The distinct effect of casamino acids on mucoidy and not capsule abundance is a critical observation, as it aligns with recent work demonstrating that capsule abundance and mucoidy are distinct from one another[11,12]. Mucoidy is now attributed to reduced CPS chain length diversity and increased uniformity, rather than simply higher capsule abundance. While we have focused here on how amino acids regulate mucoidy, we also observed that glucose suppresses mucoidy in the presence of casamino acids, indicating a complex interaction between different nutrients (Fig. 1B).

A systematic analysis of the contribution of each amino acid revealed that arginine is the key amino acid driving mucoidy (Figs. 2–3). Subsequent validation confirmed that the absence of arginine decreased mucoidy without affecting capsule abundance or growth (Fig. 2 and Supplementary Fig. 1). These data demonstrated that arginine is necessary for the regulation of *K. pneumoniae* mucoidy. Moreover, when arginine is supplemented into culture medium with glycerol as the sole carbon source, mucoidy is restored to the same level observed in M9 with all amino acids (M9+All) without altering capsule abundance (Fig. 3A, B). These data demonstrated that arginine is sufficient to positively regulate mucoidy independently of capsule abundance.

To determine how arginine regulates *K. pneumoniae* mucoidy, we investigated whether genes involved in arginine biosynthesis, degradation, or regulation regulate mucoidy. We found that the arginine regulator, ArgR, is required to stimulate *K. pneumoniae* mucoidy in response to arginine availability (Fig. 3C, D). ArgR coordinates arginine synthesis and transport, but can also regulate other genes[44–46]. Previous studies have shown that in hypervirulent *K. pneumoniae* strain NTUH-K2044, the Δ*argR* mutant exhibits decreased mucoidy and capsule abundance, with slightly reduced capsule thickness and finer filaments as visualized by electron microscopy[44]. Our KPPR1 Δ*argR* mutant mirrors the reduced mucoidy of NTUH-K2044 Δ*argR*, strengthening our conclusion that ArgR is a key mucoidy regulator (Fig. 3C). The role of ArgR in regulating mucoidy was validated by restoring mucoidy to Δ*argR* by complementing with *argR* in trans (Fig. 3E, F).

Previous work found that RmpD interacts with Wzc to reduce CPS chain length diversity and produce the mucoid phenotype[12]. Here, we demonstrate that ArgR and arginine activate the *rmpADC* promoter and increase *rmpADC* transcription, which reduce CPS chain length diversity (Figs. 4–5)[10–12]. We identified a highly conserved ARG box in the *rmp* promoter (Fig. 7A). To test whether the ARG box is required for ArgR to activate P_{rmp} in KPPR1, we mutated eight conserved ARG box nucleotides in the P_{rmp} region. P_{rmp} activity was significantly reduced in all media conditions compared to the WT P_{rmp} vector (Fig. 7B). To test whether ArgR direct binds the P_{rmp} ARG box, a DPI-ELISA was used to examine ArgR-P_{rmp}-ARG box interactions in vitro. We observed dose-response binding of ArgR to WT P_{rmp} oligonucleotides that was completely lost with $P_{rmp\Delta ARG}$ oligonucleotides (Fig. 7C).

Furthermore, a chromosomal ΔARGbox mutant strain was significantly decreased in mucoidy across all media conditions, produced significantly less *rmpADC* transcripts, and trends toward increased CPS chain length diversity (Fig. 7D–H). This indicates that the ARG box is essential for arginine-dependent regulation of mucoidy in the native promoter. In our study, *rmpADC* transcript levels were significantly reduced in the ΔARGbox mutant (Fig. 7F). Surprisingly, this mutant exhibited a significant increase in total capsule abundance compared to WT, a phenotype not observed in the Δ*argR* mutant (Fig. 3D; Fig. 7E). This difference could be due to additional regulatory functions of ArgR, such as its role in metabolism, which could separately increase total capsule abundance. This paradox has been reported before. For instance, we previously observed that KPPR1 down-regulates *rmpADC* transcript when cultured in urine, but has sustained high levels of capsule production[11]. Although others have shown that an Δ*rmpC* mutant remains mucoid yet produces less capsule, our data showing that decreased *rmpC* transcripts are not correlated with reduced capsule abundance suggesting that the effects of RmpC on capsule abundance are likely indirect[47].

Nonetheless, the data presented here support a model that, in the presence of arginine, ArgR directly binds the P_{rmp} ARG box to positively regulate *rmpADC* and increase mucoidy. This regulatory circuit

Table 1 | Genomic characterization of clinical *Klebsiella* isolates with PathogenWatch

Feature	KPPR1	NTUH-K2044	Kp4289	Kp4585	Kp6557
Strain	*K. pneumoniae*	*K. pneumoniae*	*K. pneumoniae*	*K. pneumoniae*	*K. pneumoniae*
Sequence Type	493	23	380	380	23
K Locus	KL2	KL1	KL2	KL2	KL1
Predicted K Type	K2	K1	K2	K2	K1
O Locus	O1/O2v1	O1/O2v2	O1/O2v1	O1/O2v1	O1/O2v2
Predicted O Type	O1ab	O1ab	O1ab	O1ab	O1ab
Antibiotic Resistance	Penicillin (SHV-1)	Penicillin (SHV-11)	Penicillin (SHV-207)	Penicillin (SHV-207)	Penicillin (SHV-11)
Virulence Score	1	1	4	4	5
Hyper-mucoidy (RmpADC/*rmpA2*)	*rmp* 3; ICEKp1 / -	*rmp* 3; *ICEKp1 (truncated)* / -	*rmp* 2; KpVP-2 / -	*rmp* 2; KpVP-2 / -	*rmp* 1; KpVP-1 / *rmpA2*_8-60%
Plasmid	None	None	IncFIB(K)	IncFIB(K)	*repB*_KLEB

Italicized text denotes species names and genes. Bold text emphasizes the feature category and each strain name.

controlling mucoidy is highly conserved in hypervirulent strains (Fig. 8A). This claim is supported by our observations that two hvKp laboratory strains and three hvKp clinical isolates positively regulate mucoidy and P_{rmp} via the ARG box in response to arginine (Fig. 8A, B). This represents a promising avenue to further understand how niche-specific variations in arginine availability regulate hvKp virulence. Further understanding of ArgR-P_{rmp} interactions could identify new avenues for targeting virulence factor regulation, potentially reducing the pathogenicity of hypervirulent *K. pneumoniae*.

With a better understanding of arginine as an exogenous cue that controls hvKp mucoidy, we also sought to examine whether this regulatory function may be active in specific host niches affecting in vivo fitness. Lung infections, particularly pneumonias, are a significant cause of morbidity and mortality worldwide, with *K. pneumoniae* being a major etiological agent[48,49]. In the lungs, *K. pneumoniae* faces a complex immune environment where macrophages play a crucial role in pathogen clearance[16,49,50]. Therefore, we first examined how ArgR-dependent mucoidy regulation impacts bacterial interactions with host immune cells, specifically immortalized murine bone marrow-derived macrophages (iBMDMs). We acknowledge that iBMDMs do not fully recapitulate the behavior of primary alveolar macrophages (AMs). AMs are the first immune cells in the lung to encounter pathogens like *K. pneumoniae* during pulmonary infections, and they are specifically adapted to handle the unique microenvironment of the lung, including interactions with inhaled bacteria[50,51]. While BMDMs share many functional similarities with AMs and are a widely accepted model for macrophage activation and phagocytosis, they may not fully replicate the immune dynamics encountered in the lung tissue[51]. Despite this limitation, we observed that ArgR is required for reducing both bacterial association with and internalization of iBMDMs (Fig. 6A), suggesting that positive regulation of mucoidy by ArgR may facilitate immune evasion by reducing CPS chain length diversity. We speculate that ArgR-mediated mucoidy regulation is a key *K. pneumoniae* strategy for evading host immunity, at least during pulmonary infections. Therefore, we next evaluated the role of ArgR in bacterial fitness by performing competitive infections between WT + EV and Δ*argR* + EV in a murine model of pneumonia. The Δ*argR* + EV mutant exhibited a 2-log decrease in lung colonization ($P = 0.0008$) that was overcome when Δ*argR*+p*argR* was competed against WT + EV (1-log increase, $P = 0.0078$) (Fig. 6B). These results confirm that ArgR plays an essential role in maintaining bacterial survival and replication in lung tissue, and validate prior TnSeq and insect model infection data[11,16,17,44]. Although Δ*argR* + EV showed a slight trend towards reduced competitive fitness in the liver and spleen, this did not reach statistical significance and was not complemented by Δ*argR*+p*argR*. The 2-log defect in Δ*argR* primary site colonization (*i.e.* lung) likely confounds our ability to evaluate its role in dissemination to secondary sites. In addition, ArgR also coordinates arginine import and metabolism, while host arginine levels fluctuate due to immune responses and inflammation[23,24,52]. Therefore, the rapid clearance observed in the Δ*argR* mutant may be due to ArgR involvement in these metabolic processes, in addition to its role in mucoidy regulation. Our data agree with several previous reports, which include that low mucoidy and Δ*rmpD* (resulting in a low mucoid phenotype) increased macrophage association in *K. pneumoniae*, that Δ*argR* increased *Galleria mellonella* survival, and that in *K. pneumoniae argR::kan* was significantly outcompeted in pneumonia TnSeq and bacteremia TnSeq experiments[10,11,16,17,44]. Combined, these data suggest that arginine is a key host cue used by hvKp to optimize in vivo fitness and pathogenicity via ArgR-dependent regulation.

To examine whether arginine-dependent regulation of mucoidy could occur in different host niches, we explored how arginine concentrations vary between host fluids and tissues ex vivo and their effect on ArgR:ARG box-dependent mucoidy regulation. We found that arginine abundance is higher in healthy murine lung tissues compared to spleens and livers, while murine feces is higher compared to livers (Fig. 6C). Notably, our competitive infections revealed that the Δ*argR* mutant was only outcompeted by WT in the lungs, not spleens or livers (Fig. 6B). In human biofluids, serum contained more arginine than urine (Fig. 8C). Accordingly, hvKp are more mucoid and activate P_{rmp} when cultured in HI serum; these phenotypes require ArgR and the P_{rmp} ARG box (Fig. 8D, E). These data align with prior findings that human urine suppresses mucoidy[11]. In addition, a recent study identified ArgR as a positive regulator of the *K. pneumoniae* type VI secretion system (T6SS), which is required for gut colonization[32]. Higher arginine availability in human serum, lungs, and feces may favor *K. pneumoniae* expression of mucoidy and T6SS to increase immune evasion or colonization in those niches (Fig. 8C). Conversely, in areas with lower arginine availability, such as urine and livers, reduced hvKp mucoidy could increase bacterial binding to host cells such as bladder epithelial cells or tissue-resident macrophages[11,53,54]. For example, one study showed that hvKp can be phagocytosed by Kupffer cells in the liver, where it resists phagocyte-mediated clearance and replicates intracellularly[53]. Given that arginine concentrations are relatively low in the liver, it is plausible that reduced ArgR-dependent mucoidy in this niche facilitates bacterial uptake by resident phagocytes, thereby enabling intracellular survival.

Based on data presented here, we propose the following working model (Fig. 9). Upon bacterial uptake of arginine into the cell, ArgR binds arginine to become activated[55–57]. In addition to other regulatory targets, the activated ArgR directly binds to the P_{rmp} ARG box and activates the *rmp* promoter. This activity increases *rmpADC* transcription and RmpD then interacts with Wzc to reduce CPS chain diversity[11,12]. In the great majority of cases, arginine-ArgR represses

https://doi.org/10.1038/s41467-025-61047-y

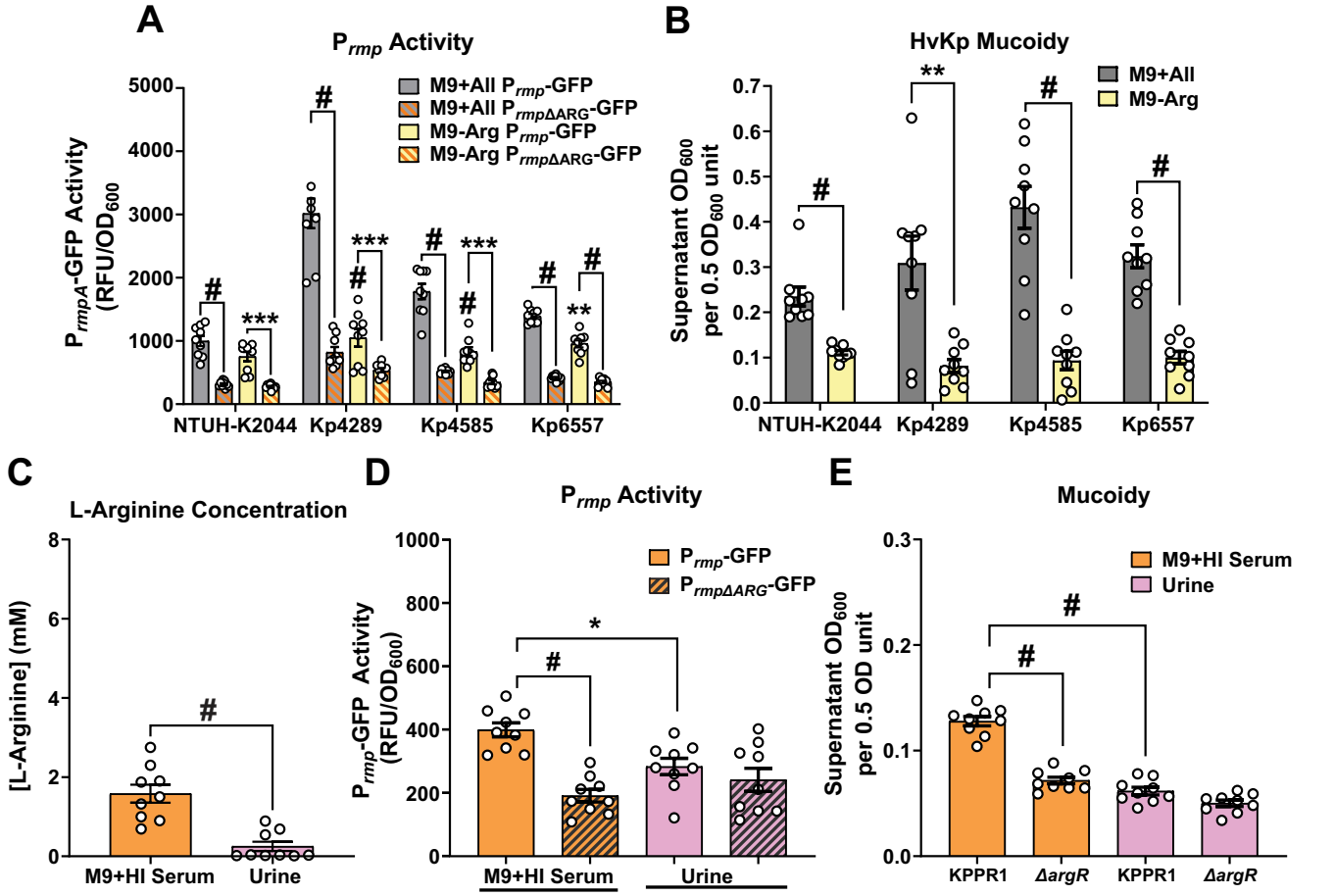

Fig. 8 | Multiple hvKp strains regulate mucoidy through the ARG box in response to arginine and host conditions. A Hypervirulent *K. pneumoniae* (hvKp) strains NTUH-K2044, Kp4289, Kp4585, and Kp6557 carrying either the P$_{rmp}$-GFP reporter plasmid or a mutated ARG box (P$_{rmpΔARG}$-GFP) were cultured in M9+All and M9-Arg. GFP expression measured promoter activity. **B** NTUH-K2044, Kp4289, Kp4585, and Kp6557 were cultured in M9+All or M9-Arg. Mucoidy was assessed by sedimentation assay. **C** 20% pooled human heat-inactivated serum was supplemented into 10x M9 salts (M9 + HI Serum). Both M9 + HI Serum and human urine samples were centrifuged to remove debris and proteinase-treated prior to arginine quantification. **D** KPPR1 carrying either the P$_{rmp\text{-}GFP}$ reporter plasmid or P$_{rmpΔARG}$-GFP was cultured in either M9 + HI Serum or sterile-filtered pooled human urine. Promoter activity was measured by GFP expression. **E** KPPR1 and Δ*argR* was cultured in M9 + HI Serum or sterile-filtered pooled human urine and mucoidy was assessed via a sedimentation assay. Data presented are the mean, and error bars represent the standard error of the mean. Statistical significance was determined in panel (**A**) using a two-way ANOVA with Tukey's post-test, while in panel (**B**) a two-tailed *t*-test was used. In panel (**C**) a two-tailed Mann-Whitney test was performed and in panels (**D** and **E**) a one-way ANOVA with Bonferroni's post-test was applied. *p*-values are displayed above each comparison: $*p < 0.05$; $**p < 0.01$; $***p < 0.001$; $\#p < 0.0001$. Exact *P*-values: (**A**), left to right above data bars: <0.0001, <0.0001, 0029; connected by lines: <0.0001, 0.0010, <0.0001, 0.0003, <0.0001, 0.0067, <0.0001, <0.0001; (**B**), left to right: <0.0001, 0.0019, <0.0001, <0.0001; (**C**), left to right: <0.0001; (**D**), left to right; <0.0001, 0.0138; (**E**), left to right: <0.0001, <0.0001. Experiments were performed > 3 independent times, each in biological triplicate ($n = 9$). Source data are provided as a Source Data file.

genes by occluding the promoter. However, there are reports of arginine-ArgR increasing gene expression by either bending the DNA or preventing the binding of another repressor protein[32,58–61]. In the context of bacterial pneumonia, we propose that arginine availability and therefore, ArgR regulation of mucoidy is a method employed by hvKp to modulate the bacterial cell surface and evade the host immune system in the lungs. This is based on our data demonstrating that ArgR blocks macrophage association and increases bacterial fitness in the lung (Fig. 6A, B).

To the best of our knowledge, this study presents the first mechanistic evidence for how ArgR regulates *K. pneumoniae* mucoidy. Our data add to existing literature, which reports that mucoidy is important for avoiding uptake by macrophages[10,11]. However, further investigation is warranted to understand where *K. pneumoniae* encounters varying arginine concentrations during colonization, invasion and infection, and how arginine-induced changes to *K. pneumoniae* cell surface properties shape the course of pathogenesis. Our preliminary data suggest that arginine availability in human urine, inactivated human serum, and murine organ homogenates varies (Figs. 6C and 8C). However, it is possible that arginine bioavailability changes under pro-inflammatory conditions. Therefore, further exploration on effects of host niche environments on mucoidy during active infection is warranted.

Adding further complexity to our understanding of hvKp mucoidy regulation in situ, we have noted that glycerol suppresses mucoidy, and other studies have demonstrated that human urine and L-glucose also suppress mucoidy[11,14]. These combined observations lead us to speculate that inputs from multiple signals are integrated in a complex regulatory cascade which fine-tunes CPS chain length diversity and, thus, mucoidy in *K. pneumoniae*. We propose that coordinated changes in cell surface properties could block clearance of bacteria by macrophages, thereby increasing bacterial survival in primary host tissues and, potentially, increasing persistence and dissemination to secondary sites. In line with this, it has been reported both mucoid and non-mucoid *K. pneumoniae* isolates were recovered from peritoneal fluid and bile in a single patient over time, suggesting

https://doi.org/10.1038/s41467-025-61047-y

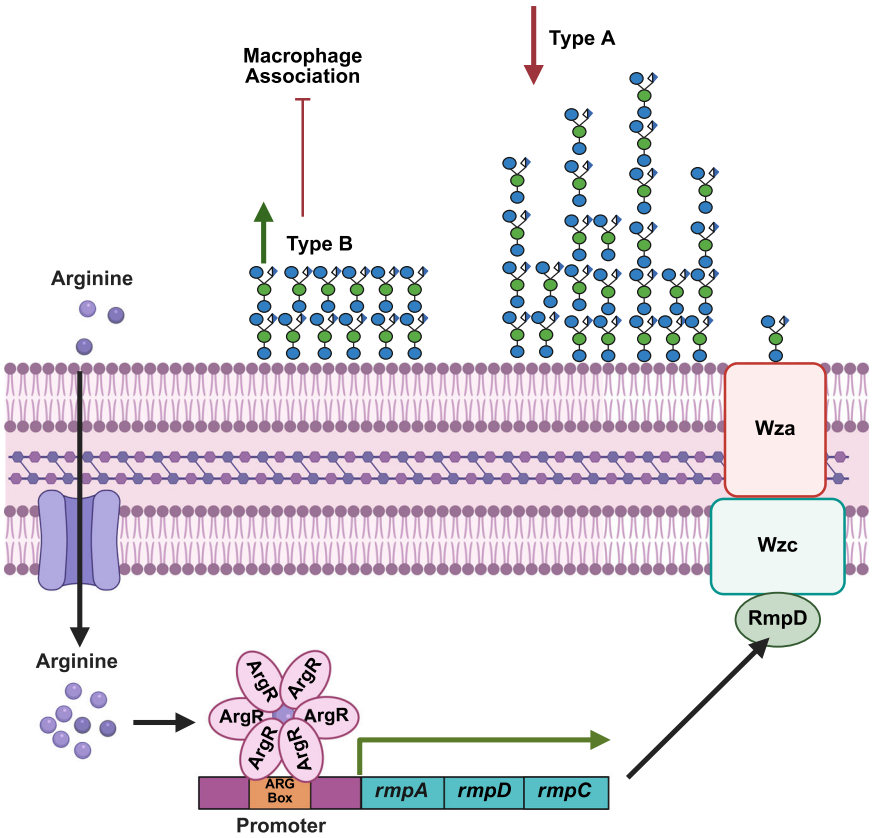

Fig. 9 | Model of *K. pneumoniae* regulation of mucoidy in response to arginine. When cultured in the presence of arginine, *K. pneumoniae* increases mucoidy without altering the total capsule abundance. When arginine is brought into the cell, the arginine regulator, ArgR, binds arginine and becomes active. The activated ArgR-arginine complex acts as a transcriptional regulator via binding to ARG boxes. The arginine-ArgR complex binds directly to the P_{rmp} ARG box and activates the *rmpADC* promoter, upregulating *rmpADC* transcription. The RmpD protein then interacts with the Wzc protein, a tyrosine autokinase that regulates high-level capsular polysaccharide (CPS) polymerization. RmpD-Wzc interactions decrease 'Type A' polysaccharide chains and increases 'Type B', which decreases CPS diversity and presents as the mucoid phenotype resulting in decreased association with macrophages. Created in BioRender. Ryan, B. (2025) https://BioRender.com/r74w727.

that dynamic regulation of mucoidy may contribute to pathogenesis by allowing the bacterium to adapt to different host environments[62]. Conversely, we speculate that the ability to switch to a non-mucoid phenotype in low-arginine environments (e.g. urine or liver) may promote adherence and persistence, without requiring the bacteria to lose capsule production entirely as has been previously reported in ST258 lineages[54]. Fully dissecting the complex regulatory network that optimizes hvKp fitness warrants further exploration as it may identify intervention points that could be targeted by anti-virulence therapies.

In summary, this study reveals the crucial role of arginine as a key signal regulating mucoidy in *K. pneumoniae* and highlights the ability of this species to fine-tune the cell-surface polysaccharides presented in response to environmental cues. We posit that *K. pneumoniae* is a 'capsule expert', with the ability to fine-tune capsule properties to optimize its niche-specific fitness. Our results indicate that the regulatory mechanisms governing the influence of arginine on mucoidy is consistent across multiple hvKp strains, underscoring its potential significance as a key driver of *K. pneumoniae* hypervirulence. Our findings also suggest that arginine signaling via ArgR may facilitate immune evasion and fitness in the lungs, expanding our understanding of factors shaping *K. pneumoniae* interactions with host immune cells. Finally, we identified a highly conserved ARG box within the *rmp* operon promoter of hypervirulent *K. pneumoniae*. Although, it is likely other nutrients, or metabolic intermediates exert regulatory control over the *rmp* locus. Ultimately, this work underscores the complex interactions between nutrient availability and bacterial virulence gene expression. Specific to hypervirulent *K. pneumoniae*, these results reveal that the mucoid phenotype is dynamic and regulated in response to environmental cues. That is, hypervirulent *K. pneumoniae* do not exist in a persistently hypermucoid state. Gaining insight into the regulatory networks that activate virulence factors in vivo is crucial for developing new targets that could reduce the pathogenicity of hypervirulent *K. pneumoniae*.

Methods

All experimental procedures comply with the ethical guidelines established by The University of Toledo. Institutional Biosafety Committee (IBC) approvals were obtained from both The University of Toledo (study number 500074-UT) and the University of Pittsburgh (PROTO202400096). All animal work was conducted adhering to the humane animal handling recommendations and approved by the University of Michigan Institutional Animal Care and Use Committee (protocol: PRO00011097). Additionally, animals were housed in accordance to the humane guidelines for animal handling, which includes a 12 h light and dark cycle, ambient temperatures between 20–26 °C, and humidity of roughly 30–35%[63]. Urine collection at the University of Toledo was approved by and performed in accordance with the Institutional Review Boards (IRB) of the University of Toledo (study number 301539-UT). Written informed consent was received from all participants prior to inclusion in the study, which included healthy female volunteers who were not menstruating, not pregnant, not diabetic, and had not taken antibiotics within 2 weeks prior to donating.

Bacterial strains and culture conditions

All the primers, oligonucleotides, bacterial strains, and plasmids described in these studies are detailed in Supplementary Data 2 and 3[11,14,16,28,30,35,36,64–66]. Bacteria were cultured in either lysogeny broth (LB) (5 g/L yeast extract, 10 g/L tryptone, 0.5 g/L NaCl) or low-iron minimal M9 base medium (6 g/L Na_2HPO4, 3 g/L KH_2PO_4, 0.5 g/L NaCl, 1 g/L NH_4Cl, 14.7 g/L $CaCl_2$, and 120.3 g/L $MgSO_4$) with the reported carbon sources (Supplementary Data 1). Cultures were shaken at 200 rpm at 37 °C, unless otherwise noted[19]. Solid medium was prepared by adding 20 g/L bacto-agar to LB medium prior to autoclaving. When appropriate, antibiotics were added at the following concentrations: kanamycin (25 μg/mL), chloramphenicol (20 μg/mL *E. coli* or 80 μg/mL *K. pneumoniae*), gentamicin (10 μg/mL), streptomycin (500 μg/mL), or hygromycin (200 μg/mL). *K. pneumoniae* KPPR1 gene deletion strains were constructed using the λ Red recombinase system and KPPR1S chromosomal point mutations were constructed using sucrose counter-selection[19,20,35]. Human urine was donated by healthy biological females who were neither menstruating, pregnant, or diabetic, nor within 2 weeks of antibiotic treatment. Urine was pooled from at least five independent donors and vacuum filtered and sterilized through 0.2 μm PES membrane[11]. Sterilized urine was stored in aliquots at −20 °C, and working volumes were stored at 4 °C.

Sedimentation assay

Hypermucoviscosity was quantified using a sedimentation assay[11,27]. A 0.5 OD_{600} unit of cultured overnight bacteria was pelleted in a 2 mL microcentrifuge tube at 1000 x *g* for 5 min. The supernatant OD_{600} was then quantified. If experimental conditions yielded an $OD_{600} < 0.5$, then a total of 0.5 OD_{600} unit of bacterial culture (exceeding 1 mL) was pelleted in a 2 mL microcentrifuge tube at 21,000 x *g* for 15 min as previously described[11]. All but 50 μL of the sample supernatant was removed, then the bacterial pellet was resuspended to 1 mL with PBS, and sedimentation efficiency was quantified after centrifugation at 1000 x *g* for 5 min.

Uronic acid quantification

For cell-associated capsular polysaccharide (CPS) quantification in all media conditions, uronic acid quantification was performed[11,27]. In brief, 250 μL of the overnight culture was mixed with either 50 μL 1% Zwittergent 3–14 (MilliporeSigma) in 100 mM citric acid buffer, pH 2 for CPS. The mixture was incubated at 50 °C for 20 min and then pelleted at 17,000 × g for 5 min. Next, 100 μL of the supernatant was transferred to 400 μL of ice-cold ethanol and incubated for 20 min on ice to precipitate CPS. Samples were rehydrated in 200 μL of ultra-pure water and then 1.2 mL of 0.0125 M sodium tetraborate in concentrated sulfuric acid was added.

Screening concentrations of arginine and phenylalanine

To identify concentrations of arginine and/or phenylalanine sufficient to restore mucoidy, we cultured KPPR1 in a 96-well plate that had wells filled with 100 μL of low-iron M9 medium supplemented with 20 mM glycerol, and which had increasing concentrations of phenylalanine and/or arginine. To prevent evaporation, the plates were wrapped with plastic wrap and incubated with shaking (200 rpm) at 37 °C for 18–20 h. The sedimentation assay was adapted to a microplate format as follows: Plates were vortexed at low speed to resuspend pellets, and the total OD_{600} was recorded. Following centrifugation at 1000 x *g* for 5 min, the upper 50 μL of supernatant was transferred to a new microplate containing 50 μL of PBS to measure the OD_{600}[30].

Growth curves

Bacterial strains were cultured at 200 rpm overnight in triplicate in 3 mL of the relevant medium in aerated 16 mL culture tubes at 37 °C. The OD_{600} was normalized to 0.001 in the reported medium. Subsequently, 100 μL of each back-diluted culture was transferred into a microplate with parafilm-wrapped edges to mitigate evaporation-related edge effects. A plate reader (EPOCH2-SN, Agilent) recorded the OD_{600} every 15 min for 16 h. The microplates were incubated at 37 °C with continuous, orbital shaking [282 cpm (3 mm)].

Molecular cloning and transformation

The oligonucleotides and plasmids employed in this study can be found in Supplementary Data 2 and 3. For generating knockouts, λ Red recombineering adapted to *K. pneumoniae* was employed[11,28–30]. To construct the plasmids, the pACYC184, pBBR1MCS5-P_{J23100} (Atum), or pVAM07 backbones and specific gene fragments were PCR amplified, gel-purified (Monarch, NEB), and assembled with NEBuilder HiFi DNA Assembly mix (NEB) for 1 h at 50 °C[67]. The resulting ligated products were transformed into chemically-competent TOP10 or Sm10 *E. coli* via heat-shock. Plasmid presence and construction was confirmed via PCR and whole plasmid sequencing. Electroporation of vectors into TOP10 *E. coli* or relevant *K. pneumoniae* strains was performed[29]. To improve hvKp transformation yield, the bacteria were recovered at 30 °C for 4 h and then at room temperature for 48 h prior to plating. Conjugation of the constructed pVAM07- ARGbox mutant into KPPR1s was performed. In brief, KPPR1s was grown alongside Sm10 λpir pVAM07-ARGbox, with the subsequent conjugated colonies passaged through both antibiotic and sucrose selection[35]. Final colonies were further validated using colony-PCR before subsequent sequencing.

Whole-genome sequencing and analysis

We performed whole-genome sequencing on the Δ*argR* and the ΔARGbox mutant strains and confirmed that the knockouts were successful, with no additional mutations detected in the genomes. In brief, genomic DNA was purified from overnight cultures by pelleting 1 mL of bacterial culture at 15,000 × *g* for 15 min at 4 °C. Samples were prepared according to the directions from the Wizard HMW DNA Extraction kit for Gram-negative Bacteria (Promega)[68]. The genomic DNA was rehydrated in DNA Rehydration Solution and Illumina sequenced (SeqCoast). Sequence variants were detected using the variation analysis pipeline on BV-BRC with the *K. pneumoniae subsp. pneumoniae* ATCC 43816 (Taxonomy ID: 1308539) as the reference genome[27]. Further analysis of the ΔARGbox mutant was performed using Benchling, where Illumina and PCR sequencing data were aligned.

Western blotting

Whole cell lysates were prepared from 27 mL of overnight culture[11]. The bacterial culture was pelleted at 21,000 x *g* for 15 min at 4 °C and samples were kept on ice. Bacterial pellets were resuspended in 500 μL of lysis buffer. The lysis buffer was prepared fresh as follows: one cOmplete Mini, EDTA-free Protease Inhibitor Cocktail tablet (Roche) and one PhosSTOP tablet (Roche) dissolved in 7 mL BugBuster (MilliporeSigma). Each sample was sonicated in two, 5 s pulses with 50% amplitude and 5 s rest between each pulse, using a Q125 sonifier (QSONICA) with a ½" diameter probe. Lysed samples were treated with nuclease for 1 h to overnight at 37 °C, 200 rpm. The nuclease was prepared fresh (4.9 mg ribonuclease A [Worthington] and 1 mg deoxyribonuclease I [Worthington] in 960 μL of 1 M Tris pH 7.5, 20 μL of 1 M $CaCl_2$, and 20 μL 1 M MgCl), and 24 μL was added to 500 μL of lysate. Protein concentration was quantified with a BCA assay (Pierce). Samples were prepared at 2 μg/μL in 1× SDS loading buffer and boiled at 70 °C for 3.5 min. Of this, 20 μg of protein were resolved on 12% SDS-PAGE gels and transferred to a nitrocellulose membrane then blocked overnight with 5% BSA (ThermoFisher) in TBS. The blot was probed with 1:2,500 mouse anti-phosphotyrosine PY20 (Abcam; ab5592), then washed with TBS-T (TBS with Tween-20) and probed with 1:5000 goat anti-mouse IgG (H + L)-HRP (secondary) (SouthernBiotech; 1036-05). Blots were developed with ECL Western Blotting Substrate (Pierce) and imaged on a G:Box Imager (Syngene)[11].

Blot stripping and re-probing

Bound antibodies were stripped off the nitrocellulose membrane with fresh, mild stripping buffer for 10 min, twice. The stripping buffer was prepared at 100 mL by adding 1.5 g glycine, 0.1 g SDS, and 1 mL Tween-20 in water with the final pH adjusted to 2.2. Blots were washed twice with PBS (10 min) and then twice with TBS-T (5 min). Stripped blots were then blocked overnight with 5% BSA in TBS overnight and then re-probed with 1:2500 anti-GAPDH loading control (primary) antibody (Invitrogen) and 1:5000 goat anti-mouse IgG (H + L)-HRP (secondary) (SouthernBiotech). Blots were developed as described above[11].

Western blot quantification

Quantification of western blots was conducted using ImageJ version 1.53 K for Windows. In short, the measurement involved selecting equal areas of each phosphotyrosine-Wzc band and GAPDH band, followed by subtracting the lane background from the obtained values. The background-subtracted value for each band was normalized relative to its corresponding background-subtracted GAPDH value. The resulting ratio of the normalized values for each bacterial strain and media condition was compared to WT was plotted. The quantification presented in the graphs represents the average of at least three independent replicates.

Fluorescence reporter assay

Bacterial strains with the fluorescent reporter plasmid were cultured at 200 rpm overnight at 37 °C in triplicate, in 3 mL of the reported medium, in 16 mL aerated culture tubes. The next day, 1 mL of overnight culture was centrifuged at 21,000 x *g* for 10 min. The supernatant was discarded, and the pellet was washed twice with 1 mL of 1x sterile PBS, then centrifuged at 21,000 x *g* for 10 min. The pellet was resuspended in 1 mL of PBS by pipetting, and 300 μL of the undiluted sample was loaded into a 96-well microplate. A blank of 300 μL 1x PBS was also included. The OD_{600} of the samples and dasherGFP abundance (485 ex/528 em) were then measured using a Cytation 5 (Biotek). The transcriptional activity of the *rmp* promoter was calculated by dividing the dasherGFP fluorescence intensity by the OD_{600} for each sample.

RNA isolation and quantitative RT-PCR

Bacteria cultured overnight in low-iron M9 minimal medium, with the appropriate amino acids and 20 mM glycerol, were diluted 1:100 into the respective low-iron M9 minimal medium culture. The bacteria were cultured with aeration at 37 °C, 200 rpm for 6 h. Then, approximately 1×10^9 CFU of bacteria were mixed at a 2:1 (vol:vol) ratio of RNAProtect (Qiagen) and incubated at room temperature for 5 min. Samples were then pelleted at 5000 × *g* for 10 min and the supernatant was decanted. RNA was purified using the RNeasy mini-prep kit (Epoch) after adding 100 μL of lysozyme (15 mg/ml in TE buffer) and 10 μL of proteinase K (20 mg/mL) and incubating for 10 min at room temperature. RNA was isolated using an RNA Mini Prep Kit (Epoch) and eluted with 30 μL of RNase-free water and samples were stored at -20 °C. Genomic DNA was removed using ezDNAse (ThermoFisher) and then cDNA synthesis was performed with SuperScript IV Reverse Transcriptase (Invitrogen) on an equal amount of RNA for each sample, roughly 1 μg total. The resulting cDNA was diluted 1:50 in water and used as template for quantitative real-time PCR (qRT-PCR) in a QuantStudio 3 PCR system (Applied Biosystem) with SYBRGreen PowerUp reagent (Invitrogen). Primers for amplifying internal fragments of the *rmpD* and *gap2* genes are listed in Supplementary Data 2, with the *gap2* transcript serving as an internal control[11]. The relative fold change was calculated using the comparative threshold cycle (C_T) method[69].

CPS chain length visualization

To visualize CPS chain length, samples were separated by SDS-PAGE and detected using alcian blue staining[11,27]. In brief, 1.5 OD_{600} of bacteria cultured overnight in low-iron M9 minimal medium with the appropriate amino acids and 20 mM glycerol were transferred to a microcentrifuge tube and pelleted at 21,000 x *g* for 15 min. The bacterial pellet was washed with 1 mL of sterile 1x PBS and centrifuged again at 21,000 x *g* for 15 min and then discarded 750 μL of the supernatant without disrupting the pellet. The pelleted cells were resuspended with the remaining volume of 250 μL PBS, and then 50 μL of 3–14 Zwittergent was added and incubated at 50 °C for 20 min. Samples were then centrifuged at 17,000 × *g* for 5 min and 100 μL of upper supernatant were precipitated in 400 μL of ice-cold ethanol for 20 min. Samples were then centrifuged at 17,000 × *g* for 5 min at 4 °C and the supernatant was discarded. The pelleted cells were then resuspended with 200 μL of ultra-pure water and placed at 37 °C for 30 min. To prepare the samples for SDS-PAGE, 75 μL of the sample was added to 25 μL of 4x SDS loading buffer. Twenty microliters of prepared sample were loaded on a 4–15% Mini-PROTEAN TGX stain-free pre-cast gel (Bio-Rad) with 20 μL of Precision Plus All Blue standard (Bio-Rad). The polysaccharides were electrophoresed for 4.5 h at 300 V on ice at 4 °C. After electrophoresis, the gel was washed in 200 mL ultrapure water for 10 min, a total of five times. It was then stained in 0.1% Alcian blue stain (0.1% wt/vol ThermoFisher Alcian Blue 8 GX in stain base solution) for 1 h with rocking. Stain base solution was prepared as 40% ethanol and 60% 20 mM sodium acetate, pH 4.75. After staining, the gel was de-stained in stain base solution overnight with rocking and then stained using Pierce Silver Stain Kit (ThermoFisher) and imaged on a Syngene G:box using the visible protein setting.

CPS chain length quantification

Quantification of the stained gels was conducted using ImageJ version 1.53 K for Windows. In brief, equal areas of the entire lane were selected and then the lane background was subtracted from the obtained values. To account for gel-to-gel variability, the control and experimental values are derived from the same gel and comparisons are only made to samples within the same gel. The quantification presented in the graphs represents the $\log_2$ fold change relative to the control of three independent gels.

Macrophage association and internalization assay

Immortalized macrophage cells derived from WT mice (BEI Resources #NR-9456) were maintained in DMEM medium with L-glutamine, 4.5 g/L glucose and sodium pyruvate (Corning) supplemented with 10% heat-inactivated fetal calf serum (Corning), 100 U/mL penicillin, and 100 μg/mL streptomycin in an atmosphere of 5% CO_2[30]. Cells were checked for confluency (~ 3×10^5 cells/well) in 24-well tissue culture dishes and were then washed with 1 mL of DPBS[30]. Then, 1 mL of 3×10^6 CFU/mL bacteria (MOI 10) in unmodified DMEM medium was added to each well. The 24-well tissue culture plate with samples were spun at 500 rpm (54 × *g*) for 5 min to bring the bacteria in contact with the macrophages and then incubated at 37 °C, 5% CO_2 for 2 h, followed by an incubation on ice for 1 h after adding 1 μL of gentamicin (100 μg/mL) treatment for internalization. Samples were washed three times with sterile 1x PBS and lysed with 1 mL of 0.2% Triton-X100 in PBS for 5 min on a rocker. Input and cell-associated bacterial counts were determined by serial dilution and CFU enumeration on LB agar.

Murine pneumonia model

This study was performed using 7–10 week-old C57BL/6 female and male mice (Jackson Laboratory, Bar Harbor, ME). Overnight LB cultures of *K. pneumoniae*, with the appropriate antibiotics, were centrifuged, resuspended, and adjusted to the proper concentration in PBS[70]. Mice were anesthetized using isoflurane and a total 1×10^6 CFU *K. pneumoniae* in a 50 μL volume (1:1 ratio of WT:mutant) was administered retropharyngeally. Twenty-four hours postinfection, mice were euthanized by carbon dioxide asphyxiation prior to collection of lungs, spleen, and liver. Organs were homogenized in sterile PBS, serially

diluted and CFU enumerated on LB agar with appropriate antibiotics (WT = Cm^R, mutant = Cm^RKm^R). The competitive index was defined as CFU from (mutant output/WT output)/(mutant input/WT input). In this study, sex was considered in the experimental design, with both male and female mice included. Specifically, KPPR1 + EV:Δ*argR* + EV included $n = 5$ males and $n = 3$ females, while KPPR1 + EV:Δ*argR*+p*argR* included $n = 5$ males and $n = 2$ females. Due to the small sample size of females in the KPPR1ev:Δ*argR*+p*argR* group, statistical comparisons based on sex were not feasible, so no direct sex-based statistical analyses were performed. Instead, the data were displayed by open symbols (for males) and half-filled symbols (for females) in all relevant data. Disaggregated data for sex are available in the source data files, with the overall numbers being $n = 10$ males and $n = 5$ females across both groups.

ArgR protein purification

BL21(DE3) carrying pET28a-*argR* was grown overnight in LB with 50 μg/mL of kanamycin, then sub-cultured into 200 mL of expression media (LB, 50 μg/mL kanamycin, and 10.3 μL of Antifoam A [Sigma-Aldrich])[32]. The culture was then grown at 37 °C with constant shaking (200 rpm) until they reached ~0.5 OD_{600}. Then 1 mL of 100 mM Isopropyl ß-D-1-thiogalactopyranoside (IPTG) was added and the culture was placed at room temperature for 4–5 h with constant shaking for protein expression. The culture was then centrifuged at max speed for 15 min to collect the bacteria, and the pellet was weighed and stored at -80 °C. Bacterial pellets were resuspended in a lysis buffer (IMAC buffer [NEB], 5% glycerol, 0.5% Triton X-100, 10 mM 2-mercaptoethanol, 2 mg/ml lysozyme, and 50 μl/g Protease Inhibitor Cocktail [SigmaAldrich]; 5 mL per 1 gram of pellet), incubated at room temperature for 5 min, then chilled on ice for 10 min. Bacterial suspensions were sonicated 10X using a Q125 sonifier (QSONICA) with a ½" diameter probe (30 s pulses with 50% amplitude and 30 s rest between each pulse), then centrifuged (12,000 × *g*, 15 min, 4 °C). The supernatant was passed through a 0.45 μm filter. Protein was then purified using the NEBExpress Ni Spin Column Kit (NEB) with a high-salt wash buffer (50 mM Imidazole, 500 mM NaCl, 50 mM NaH2PO4, pH 8) to reduce non-specific binding. The final elution buffer was exchanged for a storage buffer (10 mM Tris-HCl, 100 mM NaCl, 5% glycerol, pH 8) by dialysis using a 10 K MWCO Slide-A-Lyzer® MINI (Thermo Scientific). For confirming protein purity, an aliquot of the elution was run on 12% SDS-PAGE gel and stained with Coomassie Brilliant Blue (Thermo Scientific). Protein concentration was measured via Bradford assay.

DNA protein interaction (DPI) ELISA

Biotinylated DNA oligonucleotides (2 pmol) containing the ARG box in the *rmpADC* promoter or the mutated ARG box were bound to a streptavidin-coated plates by incubating for 2 h at room temperature with rocking[32]. After binding the DNA oligonucleotides, wells were washed four times with 200 μL of TBS-T. Then 150 μL of 5% non-fat milk in PBS blocking solution was added to the wells and incubated at room temperature for 2 h. The purified His-tagged ArgR protein (5 μg) was serially diluted at 1:1 ratios in blocking buffer (60 μL/well) and incubated for 1 h. After protein incubation, the wells were washed four times with 200 μL of TBS-T. Anti-His mouse monoclonal HRP conjugate antibody (Southern Biotech; 4603-05) was diluted 1:1000 in PBS and added to the wells (60 μL/well) and incubated for 1 h at room temperature. After antibody incubation, the wells were washed two times with 200 μL of PBS-T and two times with 200 μL of PBS. To develop, 100 μL/ well of 1-Step Slow TMB-Elisa Substrate Solution (Thermo Scientific) until a color change occurred, the reaction was stopped with 100 μL per well of 0.18 M H_2SO_4, and the OD_{450} was then measured.

Arginine concentration assay

Arginine concentrations were evaluated using the EnzyChrom™ L-Arginine Assay Kit (BioAssay Systems). To measure arginine concentrations in murine lungs, spleens, and livers they were first homogenized in PBS (3x volume of the sample for lungs and spleen, 2x for livers) and then centrifuged for 5 min at 18,407 *x g* to remove any debris. For arginine concentrations in M9 + HI Serum, pooled human complement serum (Innovative Research) was heat-inactivated at 56–58 °C for 1 h prior to being supplemented into low iron minimal M9 medium. All murine and human samples were then proteinase-treated samples with proteinase K (20 mg/mL) overnight at 37 °C and then heat-inactivated at 95 °C for 7 min. Samples were then centrifuged for 5 min at 18,407 *x g* to remove solid debris. Then 10 μL of sample were loaded onto a 96-well plate in triplicate for blank and sample. In addition, an internal standard (10 μL of 0.5 mM arginine with the sample) was loaded. To the sample and internal standard wells, 40 μL of the working solution (42 μL Assay Buffer, 1 μL Enzyme Mix, and 0.5 μL Mn Solution, 42 μL was made according to kit instructions) containing the enzyme mix is added. 40 μL of the working solution without the enzyme mix added was added to the blank wells. The plate was incubated at 37 °C for 30 min and then the reaction was stopped with 150 μL of the urea reagent. The absorbance (OD_{450}) is immediately measured (time 0) and then measured again after 60 min. The arginine concentration is calculated by taking the difference in OD_{450} between the sample and the sample blank (OD_{450} of sample at 60 min minus OD_{450} of sample at time 0) and subtracting the difference in OD between the internal standard and the sample ($OD_{450}$of internal standard at 60 min minus OD_{450} of internal standard at time 0). This value is then multiplied by the sample dilution factor (n) and 0.5 to get the final concentration of arginine.

Genetic characterization of hvKp clinical isolates and ARG box alignment

Raw sequence reads of Kp4289 (SRA accession: SRR19095630), Kp4585 (SRA accession: SRR19095615), and Kp6557 (SRA accession: SRR18982352) from the NCBI database were assembled using PATRIC (https://www.bv-brc.org)[36]. Assembled sequences, including NTUH-K2044, were uploaded to Pathogenwatch (https://pathogen.watch/) for species identification and identification of the *rmp* operon[37–43]. All other *K. pneumoniae* genomes were downloaded from NCBI on November 26th, 2023. Genomes were included in this study if they met the following criteria: the BioSample metadata for "host" was listed as "Homo sapiens", "Homo sapiens sapiens", or "homo", the BioSample metadata for "isolation source" grouped into "urine", "respiratory", "blood", or "gastrointestinal" categories, and the genome had a BioSample "collection date" and "geolocation". Genomes were characterized using Kleborate v2.4.1 and those with intact *rmpADC* loci ($n = 1,572$) underwent further analysis[71]. These genomes were compared to KPPR1 ARG box reference sequence (ACTTTTTATTGTTATTGATTGAATTTTTATTCATTAAAAATTGTAACAAACGACGTTC) using Geneious v2023.1.1 (https://www.geneious.com). The diversity of the ARG box and surrounding region was visualized using WebLogo v3.7.9[72,73].

Statistics

All replicates represent biological replicates, except for qPCR and DPI-ELISA which included technical replicates that were experimentally tested at least three independent times. All statistical analyses were computed in Prism 10 (GraphPad Software, La Jolla, CA, USA). For experiments comparing multiple groups on two independent factors, significance was calculated using two-way ANOVA with a Tukey or Bonferroni posttest to compare specific groups. For experiments comparing three or more groups on one independent factor, significance was calculated one-way ANOVA either a Dunnett, Bonferroni, or Tukey posttest. A *t*-test was used for comparing two groups, while a one sample *t*-test was used when comparing groups to a hypothetical value of 0. Results were considered significant if the *P*-value was less than or equal to 0.05. All box plots included in this study display individual data points, the horizontal line indicates the median, the

box bounds indicate the minima (25th percentile) and maxima (75th percentile), and whiskers denote the full range. All data presented are the mean, and error bars represent the standard error of the mean.

Reporting summary

Further information on research design is available in the Nature Portfolio Reporting Summary linked to this article.

Data availability

The sequencing data generated in this study have been deposited in the NCBI Sequence Read Archive (SRA) under accession code PRJNA1255067. Previously published raw sequencing data analyzed in this study are available in the NCBI SRA under the following accession numbers: SRR19095630 (Kp4289), SRR19095615 (Kp4585), and SRR18982352 (Kp6557). All other data generated in this study are provided in the Supplementary Information 'Source Data' file. Source data are provided with this paper.

References

1. Ikuta, K. S. et al. Global mortality associated with 33 bacterial pathogens in 2019: a systematic analysis for the Global Burden of Disease Study 2019. *Lancet* **400**, 2221–2248 (2022).
2. Lan, P., Jiang, Y., Zhou, J. & Yu, Y. A global perspective on the convergence of hypervirulence and carbapenem resistance in *Klebsiella pneumoniae*. *J. Glob. Antimicrob. Resist.* **25**, 26–34 (2021).
3. Russo, T. A. & Marr, C. M. Hypervirulent *Klebsiella pneumoniae*. *Clin. Microbiol. Rev.* **287**, 283–300 (2019).
4. Russo, T. A. et al. Identification of biomarkers for differentiation of hypervirulent *Klebsiella pneumoniae* from classical *K. pneumoniae*. *J. Clin. Microbiol.* **56**, e00776-18 (2018).
5. Dai, P. & Hu, D. The making of hypervirulent *Klebsiella pneumoniae*. *J. Clin. Lab Anal.* **36**, e24743 (2022).
6. Chang, D., Sharma, L., Dela Cruz, C. S. & Zhang, D. Clinical epidemiology, risk factors, and control strategies of *Klebsiella pneumoniae* infection. *Front. Microbiol.* **12**, 750662 (2021).
7. Fang, C. T., Yi, W. C., Shun, C. T. & Tsai, S. F. DNA adenine methylation modulates pathogenicity of *Klebsiella pneumoniae*genotype K1. *J. Microbiol. Immunol. Infect.* **50**, 471–477 (2017).
8. Choby, J. E., Howard-Anderson, J. & Weiss, D. S. Hypervirulent *Klebsiella pneumoniae* – clinical and molecular perspectives. *J. Intern. Med.* **287**, 283–300 (2020).
9. Piperaki, E. T., Syrogiannopoulos, G. A., Tzouvelekis, L. S. & Daikos, G. L. *Klebsiella pneumoniae*: Virulence, Biofilm and Antimicrobial Resistance. *Pediatr. Infect. Dis. J.* **36**, 1002–1005 (2017).
10. Walker, K. A., Treat, L. P., Sepúlveda, V. E. & Miller, V. L. The small protein RmpD drives hypermucoviscosity in *Klebsiella pneumoniae*. *mBio* **11**, e01750-20 (2020).
11. Khadka, S. et al. Urine-mediated suppression of *Klebsiella pneumoniae* mucoidy is counteracted by spontaneous Wzc variants altering capsule chain length. *Msphere* **8**, e00288–00223 (2023).
12. Ovchinnikova, O. G. et al. Hypermucoviscosity regulator RmpD interacts with Wzc and controls capsular polysaccharide chain length. *mBio* **14**, e0080023 (2023).
13. Le, M. N. et al. Genomic epidemiology and temperature dependency of hypermucoviscous *Klebsiella pneumoniae* in Japan. *Microb. Genom.* **8**, mgen000827 (2022).
14. Hudson, A. W., Barnes, A. J., Bray, A. S., Ornelles, D. A. & Zafar, M. A. *Klebsiella pneumoniae* L-fucose metabolism promotes gastrointestinal colonization and modulates Its virulence determinants. *Infect. Immun.* **90**, e0020622 (2022).
15. Carfrae, L. A. & Brown, E. D. Nutrient stress is a target for new antibiotics. *Trends Microbiol.* **31**, 571–585 (2023).
16. Bachman, M. A. et al. Genome-wide identification of *Klebsiella pneumoniae* fitness genes during lung infection. *MBio* **6**, e00775 (2015).
17. Holmes, C. L. et al. *Klebsiella pneumoniae* causes bacteremia using factors that mediate tissue-specific fitness and resistance to oxidative stress. *PLoS Pathog.* **19**, e1011233 (2023).
18. Alteri, C. J. & Mobley, H. L. T. Metabolism and fitness of urinary tract pathogens. *Microbiol. Spectr.* https://doi.org/10.1128/microbiolspec.MBP-0016-2015 (2015).
19. Murdoch, C. C. & Skaar, E. P. Nutritional immunity: the battle for nutrient metals at the host-pathogen interface. *Nat. Rev. Microbiol.* **20**, 657–670 (2022).
20. Gogoi, M., Datey, A., Wilson, K. T. & Chakravortty, D. Dual role of arginine metabolism in establishing pathogenesis. *Curr. Opin. Microbiol.* **29**, 43–48 (2016).
21. Menezes-Garcia, Z., Kumar, A., Zhu, W., Winter, S. E. & Sperandio, V. L-Arginine sensing regulates virulence gene expression and disease progression in enteric pathogens. *Proc. Natl. Acad. Sci. USA* **117**, 12387–12393 (2020).
22. Reitzer, L. & Zimmern, P. Rapid growth and metabolism of uropathogenic *Escherichia coli* in relation to urine composition. *Clin. Microbiol. Rev.* **33**, e00101-19 (2019).
23. Paulson, N. B. et al. The arginine decarboxylase pathways of host and pathogen interact to impact inflammatory pathways in the lung. *PLoS One* **9**, e111441 (2014).
24. Palmer, K. L., Aye, L. M. & Whiteley, M. Nutritional cues control *Pseudomonas aeruginosa* multicellular behavior in cystic fibrosis sputum. *J. Bacteriol.* **189**, 8079–8087 (2007).
25. Wong Fok Lung, T. et al. *Klebsiella pneumoniae* induces host metabolic stress that promotes tolerance to pulmonary infection. *Cell Metab.* **34**, 761–774.e769 (2022).
26. Lin, C. T. et al. Fur regulation of the capsular polysaccharide biosynthesis and iron-acquisition systems in *Klebsiella pneumoniae* CG43. *Microbiol. (Read.)* **157**, 419–429 (2011).
27. Khadka, S., Ring, B. E., Pariseau, D. A. & Mike, L. A. Characterization of *Klebsiella pneumoniae* extracellular polysaccharides. *Curr. Protoc.* **3**, e937 (2023).
28. Datsenko, K. A. & Wanner, B. L. One-step inactivation of chromosomal genes in *Escherichia coli* K-12 using PCR products. *Proc. Natl. Acad. Sci. USA* **97**, 6640–6645 (2000).
29. Ring, B. E., Khadka, S., Pariseau, D. A. & Mike, L. A. Genetic manipulation of *Klebsiella pneumoniae*. *Curr. Protoc.* **3**, e912 (2023).
30. Mike, L. A. et al. A systematic analysis of hypermucoviscosity and capsule reveals distinct and overlapping genes that impact *Klebsiella pneumoniae* fitness. *PLoS Pathog.* **17**, e1009376 (2021).
31. Walker, K. A. & Miller, V. L. The intersection of capsule gene expression, hypermucoviscosity and hypervirulence in *Klebsiella pneumoniae*. *Curr. Opin. Microbiol.* **54**, 95–102 (2020).
32. Bray, A. S. et al. *Klebsiella pneumoniae* employs a type VI secretion system to overcome microbiota-mediated colonization resistance. *Nat. Commun.* **16**, 940 (2025).
33. Ramirez, M. S., Traglia, G. M., Lin, D. L., Tran, T. & Tolmasky, M. E. Plasmid-mediated antibiotic resistance and virulence in Gram-negatives: the *Klebsiella pneumoniae* paradigm. *Microbiol. Spectr.* **2**, 1–15 (2014).
34. Brand, L. H., Kirchler, T., Hummel, S., Chaban, C. & Wanke, D. DPI-ELISA: a fast and versatile method to specify the binding of plant transcription factors to DNA in vitro. *Plant Methods* **6**, 25 (2010).
35. Van Allen, M. E., Chandrashekarappa, D. G., Bina, X. R. & Bina, J. E. New vectors and optimal conditions for allelic exchange in hypervirulent *Klebsiella pneumoniae*. *J. Microbiol. Methods* **228**, 107070 (2025).
36. Vornhagen, J. et al. Combined comparative genomics and clinical modeling reveals plasmid-encoded genes are independently associated with *Klebsiella* infection. *Nat. Commun.* **13**, 4459 (2022).
37. Bayliss, S. C. et al. The promise of whole genome pathogen sequencing for the molecular epidemiology of emerging aquaculture pathogens. *Front. Microbiol.* **8**, 121 (2017).

38. Harris, S. R. et al. Public health surveillance of multidrug-resistant clones of *Neisseria gonorrhoeae* in Europe: a genomic survey. *Lancet Infect. Dis.* **18**, 758–768 (2018).
39. Sánchez-Busó, L. et al. Europe-wide expansion and eradication of multidrug-resistant *Neisseria gonorrhoeae* lineages: a genomic surveillance study. *Lancet Microbe* **3**, e452–e463 (2022).
40. Gladstone, R. A. et al. Visualizing variation within global pneumococcal sequence clusters (GPSCs) and country population snapshots to contextualize pneumococcal isolates. *Microb. Genom.* **6**, e000357 (2020).
41. Mitchell, C. et al. Globetrotting strangles: the unbridled national and international transmission of *Streptococcus equi* between horses. *Microb. Genom.* **7**, mgen000528 (2021).
42. Argimón, S. et al. A global resource for genomic predictions of antimicrobial resistance and surveillance of *Salmonella Typhi*at pathogenwatch. *Nat. Commun.* **12**, 2879 (2021).
43. Li, X. et al. Comparing genomic variant identification protocols for *Candida auris*. *Microb. Genom.* **9**, mgen000979 (2023).
44. Dorman, M. J., Feltwell, T., Goulding, D. A., Parkhill, J. & Short, F. L. The capsule regulatory network of *Klebsiella pneumoniae* defined by density-TraDISort. *mBio* **9**, 01863–01818 (2018).
45. Cho, B. K., Federowicz, S., Park, Y. S., Zengler, K. & Palsson, B. Deciphering the transcriptional regulatory logic of amino acid metabolism. *Nat. Chem. Biol.* **8**, 65–71 (2011).
46. Barrientos-Moreno, L., Molina-Henares, M. A., Ramos-González, M. I. & Espinosa-Urgel, M. Role of the transcriptional regulator ArgR in the connection between arginine metabolism and c-di-GMP signaling in *Pseudomonas putida*. *Appl Environ. Microbiol.* **88**, e0006422 (2022).
47. Walker, K. A. et al. A *Klebsiella pneumoniae* regulatory mutant has reduced capsule expression but retains hypermucoviscosity. *mBio* **10**, e00089-19 (2019).
48. Cortés, G., Alvarez, D., Saus, C. & Albertí, S. Role of lung epithelial cells in defense against *Klebsiella pneumoniae* pneumonia. *Infect. Immun.* **70**, 1075–1080 (2002).
49. Holmes, C. L., Anderson, M. T., Mobley, H. L. T. & Bachman, M. A. Pathogenesis of Gram-negative bacteremia. *Clin. Microbiol. Rev.* **34**, e00234-20 (2021).
50. Broug-Holub, E. et al. Alveolar macrophages are required for protective pulmonary defenses in murine *Klebsiella pneumoniae*: elimination of alveolar macrophages increases neutrophil recruitment but decreases bacterial clearance and survival. *Infect. Immun.* **65**, 1139–1146 (1997).
51. Woods, P. S. et al. Tissue-resident alveolar macrophages do not rely on glycolysis for LPS-induced inflammation. *Am. J. Respir. Cell Mol. Biol.* **62**, 243–255 (2020).
52. Charlier, D. & Bervoets, I. Regulation of arginine biosynthesis, catabolism and transport in *Escherichia coli*. *Amino Acids* **51**, 1103–1127 (2019).
53. Hoh, C. H., Tan, Y. H. & Gan, Y. H. Protective role of Kupffer cells and macrophages in *Klebsiella pneumoniae*-induced liver abscess disease. *Infect. Immun.* **87**, e00369–19 (2019).
54. Ernst, C. M. et al. Adaptive evolution of virulence and persistence in carbapenem-resistant *Klebsiella pneumoniae*. *Nat. Med.* **26**, 705–711 (2020).
55. Torres Montaguth, O. E., Bervoets, I., Peeters, E. & Charlier, D. Competitive repression of the *artPIQM* operon for arginine and ornithine transport by arginine repressor and leucine-responsive regulatory protein in *Escherichia coli*. *Front Microbiol* **10**, 1563 (2019).
56. Cho, S. et al. The architecture of ArgR-DNA complexes at the genome-scale in *Escherichia coli*. *Nucleic Acids Res.* **43**, 3079–3088 (2015).
57. Cherney, L. T., Cherney, M. M., Garen, C. R., Lu, G. J. & James, M. N. Crystal structure of the arginine repressor protein in complex with the DNA operator from *Mycobacterium tuberculosis*. *J. Mol. Biol.* **384**, 1330–1340 (2008).
58. Kiupakis, A. K. & Reitzer, L. ArgR-independent induction and ArgR-dependent superinduction of the *astCADBE* operon in *Escherichia coli*. *J. Bacteriol.* **184**, 2940–2950 (2002).
59. Lu, C. D., Winteler, H., Abdelal, A. & Haas, D. The ArgR regulatory protein, a helper to the anaerobic regulator ANR during transcriptional activation of the *arcD* promoter in *Pseudomonas aeruginosa*. *J. Bacteriol.* **181**, 2459–2464 (1999).
60. Lu, C. D. & Abdelal, A. T. Role of ArgR in activation of the ast operon, encoding enzymes of the arginine succinyltransferase pathway in *Salmonella typhimurium*. *J. Bacteriol.* **181**, 1934–1938 (1999).
61. Maghnouj, A., de Sousa Cabral, T. F., Stalon, V. & Vander Wauven, C. The *arcABDC* gene cluster, encoding the arginine deiminase pathway of *Bacillus licheniformis*, and its activation by the arginine repressor *argR*. *J. Bacteriol.* **180**, 6468–6475 (1998).
62. Lee, H. et al. Evolution of *Klebsiella pneumoniae* with mucoid and non-mucoid type colonies within a single patient. *Int J. Med. Microbiol.* **309**, 194–198 (2019).
63. (US) NRC. *Guide for the Care and Use of Laboratory Animals* 8th edn, Vol. 246 (National Academies Press, 2011).
64. Broberg, C. A., Wu, W., Cavalcoli, J. D., Miller, V. L. & Bachman, M. A. Complete genome sequence of *Klebsiella pneumoniae* strain ATCC 43816 KPPR1, a rifampin-resistant mutant commonly used in animal, genetic, and molecular biology studies. *Genome Announc.* **2**, e00924-14 (2014).
65. Wu, K. M. et al. Genome sequencing and comparative analysis of *Klebsiella pneumoniae* NTUH-K2044, a strain causing liver abscess and meningitis. *J. Bacteriol.* **191**, 4492–4501 (2009).
66. Palacios, M., Broberg, C. A., Walker, K. A. & Miller, V. L. A Serendipitous mutation reveals the severe virulence defect of a *Klebsiella pneumoniae fepB* mutant. *mSphere* **2**, e00341-17 (2017).
67. Anderson, M. T. et al. Identification of distinct capsule types associated with *Serratia marcescens* infection isolates. *PLoS Pathogens* **18**, e1010423 (2022).
68. Pariseau, D. A., Ring, B. E., Khadka, S. & Mike, L. A. Cultivation and genomic DNA extraction of *Klebsiella pneumoniae*. *Curr. Protoc.* **4**, e932 (2024).
69. Schmittgen, T. D. & Livak, K. J. Analyzing real-time PCR data by the comparative C(T) method. *Nat. Protoc.* **3**, 1101–1108 (2008).
70. Holmes, C. L. et al. The ADP-heptose biosynthesis enzyme GmhB is a conserved Gram-negative bacteremia fitness factor. *Infect. Immun.* **90**, e0022422 (2022).
71. Lam, M. M. C. et al. A genomic surveillance framework and genotyping tool for *Klebsiella pneumoniae* and its related species complex. *Nat. Commun.* **12**, 4188 (2021).
72. Schneider, T. D. & Stephens, R. M. Sequence logos: a new way to display consensus sequences. *Nucleic Acids Res.* **18**, 6097–6100 (1990).
73. Crooks, G. E., Hon, G., Chandonia, J. M. & Brenner, S. E. WebLogo: a sequence logo generator. *Genome Res.* **14**, 1188–1190 (2004).

Acknowledgements

The following reagent was obtained through BEI Resources, NIAID, NIH: Macrophage Cell Line Derived from Wild-Type Mice, NR-9456. We thank Drs. Neal Hammer and Paige Kies for guidance on supplementing amino acids into a defined medium. We thank Drs. Matthew Parsek and Xuhui Zheng for the pBBR1 plasmid backbone. We thank Drs. Ammar Zafar, Maidul Islam, and Andrew Bray for the DPI ELISA protocol and guidance during protein purification. We thank Dr. Jim Bina and Mia Van Allen for reagents and advice for generating chromosomal point mutations. We thank members of the Mike lab and Department of Medical Microbiology and Immunology at the University of Toledo for critical feedback and for sharing technical expertise and resources, especially Emily Kinney, Krista Pettee, Drs. R. Mark Wooten, Jason Huntley, Jennifer Hill, and

Robert Blumenthal. Research reported in this publication was supported by the University of Toledo College of Medicine and Life Sciences, Department of Medicine at the University of Pittsburgh School of Medicine, American Heart Association 23CDA1056712 (L.A.M.), K22 AI145849 (L.A.M.), R35 GM150588 (L.A.M.), and K99A1175481 (C.L.H.) from the National Institutes of Health. The content is solely the responsibility of the authors and does not necessarily represent the official views of the American Heart Association or the National Institutes of Health.

Author contributions

B.E.R. and L.A.M. conceived the project. B.E.R., G.E.S., C.L.H., D.J.S., and E.G.M. performed the experiments. B.E.R. drafted the manuscript with input from L.A.M., C.L.H., and M.A.B. B.E.R., C.L.H., D.V.T. and L.A.M. designed the experiments. S.K, D.J.S. and G.E.S. contributed construction of plasmids. L.A.M. supervised and guided the project. All authors reviewed, edited and approved the manuscript.

Competing interests

The authors declare no competing interests.

Additional information

Supplementary information The online version contains supplementary material available at https://doi.org/10.1038/s41467-025-61047-y.

Correspondence and requests for materials should be addressed to Laura A. Mike.

Peer review information *Nature Communications* thanks Renee Fleeman, and the other, anonymous, reviewers for their contribution to the peer review of this work. A peer review file is available.